Fall 2012

Fabrication of complex ceramic parts with sacrificial material using freeze-form extrusion fabrication

Diego Armando Garcia Montaño

Recommended Citation

FABRICATION OF COMPLEX CERAMIC PARTS WITH SACRIFICIAL

MATERIAL USING FREEZE-FORM EXTRUSION FABRICATION

by

DIEGO ARMANDO GARCIA MONTAÑO

A THESIS

Presented to the Faculty of the Graduate School of the

MISSOURI UNIVERSITY OF SCIENCE AND TECHNOLOGY

In Partial Fulfillment of the Requirements for the Degree

MASTER OF SCIENCE IN MANUFACTURING ENGINEERING

2012

Approved by

Ming C. Leu, Advisor
Robert G. Landers
Gregory E. Hilmas

ABSTRACT

An additive manufacturing process called Freeze-form Extrusion Fabrication (FEF) was developed in this study to fabricate complex ceramic parts that require the use of sacrificial materials. The aqueous paste of alumina (Al_2O_3) was used as the main material, with solids loadings as high as 50 vol. % and water as the main liquid medium. Methyl cellulose, with a 10 vol. % solids loading and 90 vol. % water content, was used as the sacrificial material. The freeze-form extrusion machine has multiple extruders (extrusion devices) capable of fabricating parts from multiple materials without mixing them. The dynamic process of extruding alumina and methyl cellulose was characterized using an empirical first-order model with the ram velocity as the input and the extrusion force as the output for alumina and methyl cellulose pastes. After modeling the dynamics of extruding alumina and methyl cellulose pastes, a General Tracking Controller (GTC) was applied in order to achieve a consistent paste deposition with a constant extrusion rate for extrusion of both the part and sacrificial materials. This controller also performs Extrusion on Demand (EOD), which starts and stops the paste extrusion on demand and facilitates the switching process between different materials while fabricating complex parts. Freeze-drying was used to remove the water content after building parts from alumina and methyl cellulose pastes. Finally, the parts were debinded to burn out the methyl cellulose binder and sintered to densify the ceramic part.

ACKNOWLEDGMENTS

The work presented in this thesis would not have been possible without the guidance and instruction of my advisor, Dr. Ming C. Leu. I also would like to thank my committee members for their contribution to my work, including Dr. Robert G. Landers for sharing his knowledge with me so that I could apply it to my research and Dr. Gregory E. Hilmas for his instruction and guidance.

I would like to thank Kenneth Gorman for his assistance in the machine modification and Robert J. Hirbar, Joe Boze, and Kenneth Schmid for their assistance in the machining and repair of mechanical parts. I would like to thank Mitchell Cottrell for his technical knowledge and assistance in the hardware setup.

I would like to thank my graduate and undergraduate colleagues Dr. Jeremy Watts, Brad Deuser, Hesam Zomorodi, Aaron Thornton, Max Mulholland, Ang Li, Sajeev Chirayil, Chinmay Dhapalapurkar and Krishna Kolan for their help, support, and friendship throughout my graduate work.

I would like to thank my father Ricardo, my mother Wilma Rosario, and my brothers Richi and Sergio Remy for their unconditional support and encouragement.

Finally, I would like to thank my Lord, for giving me wisdom and strength to complete my studies.

TABLE OF CONTENTS

LIST OF ILLUSTRATIONS

LIST OF TABLES

NOMENCLATURE

Symbol	Description
F	Extrusion force
V	Ram velocity
τ	Time constant
K	Gain
σ	Standard deviation
T	Sampling frequency
F_{ss}	Steady state force

1. INTRODUCTION

1.1. LITERATURE REVIEW

Ceramic materials are applied widely in aerospace, automotive, biological, and other industries [1]. Many ceramic materials, such as Al_2O_3 and ZrB_2, can survive high temperatures (up to 2000°C for alumina and 3000°C for zirconium diboride), but processing these materials for use as components is often challenging, expensive, and time-consuming. Building a ceramic part using additive manufacturing (AM) may reduce the material cost and build time for small runs and for parts with complex geometries.

Several AM processes can be used to produce ceramic parts directly. One of these, based on Fuse Deposition Modeling (FDM) developed by Stratasys [5], is called fuse deposition of ceramics (FDC) [2-6]. Stereolitography (SLA) [6], 3D Printing (3DP) [7, 8], and Selective Laser Sintering (SLS) [9, 10] also are commercialized AM techniques for fabricating mostly polymer components with limited capabilities to make ceramic parts. Research on the use of sacrificial materials in AM processes has been ongoing for the past decade [11-12]. Direct Ink Writing (DIW) of 3D ceramic structures [12] uses droplets or filament-based writing to deposit primarily ceramic materials with carbon black as the support material using a small nozzle tip. This process uses a pressure-driven micro fluidic deposition nozzle with concentrated inks composed of metallic nano-particles, sol-gel oxides, or polymers to create complex planar and 3D structures.

Freeze-form Extrusion Fabrication (FEF) is a layer-by-layer extrusion process developed by extending the technology of Rapid Freeze Prototyping (RFP) [13-15]. This

environmentally friendly process was developed for the freeform fabrication of ceramic-based components. The method is based on the deposition of ceramic pastes using water as the main liquid medium. The aqueous paste used in the FEF process is extruded by a ram extruder, and the extruded material immediately deposits on a working surface that can be moved by an X-Y table. The surface is set to a temperature designed to freeze the material as it is deposited. The ceramic solids loading can be 50 vol. % or higher. The system's process parameters and their effect on the geometry of the parts were examined in this study. 3D components were fabricated by extrusion deposition of the aqueous ceramic paste in a layer-by-layer fashion.

The process parameters required to achieve better part quality in the FEF process have been studied previously [13-17]. Huang et al. [16] showed that with a constant ram velocity, the flow rate of a ceramic-based paste is not always constant. To achieve more consistent material extrusion, an on/off feedback controller was designed and implemented. This controller used the extrusion force reading from a load cell to automatically adjust the ram velocity and maintain a constant extrusion force. Zhao et al. [17] found that due to effects such as air bubble release, agglomerate breakdown, and liquid phase migration, the ram velocity was difficult to control. Hence, an adaptive controller was designed and implemented to regulate the extrusion force. Also, the Recursive Least Squares method (RLS) was used to estimate the extrusion force model parameters during part fabrication; a low–order control scheme capable of tracking any specified general reference trajectories was designed and implemented to regulate the extrusion process, yielding very good fabrication results with parts such as ogive cones and square alumina blocks. As a summary, extensive research has been carried out

related to the FEF process; nevertheless, this AM process was never applied to build complex ceramic parts with support material.

1.2. RESEARCH CHALLENGES AND OBJECTIVES

Most existing paste extrusion based additive manufacturing systems were developed for use at room temperatures and utilize non-aqueous ceramic-based materials. Therefore, they require a large amount of binder content for part fabrication (40-50 vol. %) [9-11].

The challenge of this research was to find, using the current capabilities of the FEF process, a new method of fabricating complex ceramic parts using support material in freezing conditions. Choosing a suitable support material for the process was challenging due to the desire to prepare the material in an aqueous-based solution with low binder content in order to keep the process environmentally friendly. The use of support materials during the FEF process was not investigated in previous studies [16-18]. Therefore, the research objectives included finding a suitable support material to use with alumina paste during the freeze-form extrusion fabrication process. A single-extruder FEF machine was modified to a multiple-extruder machine capable of extruding different materials. This FEF process with multiple extruders is capable of building parts with different types of features, e.g., internal holes, overhangs, and using multiple materials.

After finding the adequate support material, mathematical models of the pastes' dynamics were developed based on experiments with both alumina and sacrificial materials. In order to achieve a constant extrusion rate by controlling the force extrusion

of the materials while fabricating the part, a feedback force controller was applied. The force controller also was able to control the starting and stopping of the paste extrusion of the main and support materials. This ability is important because it facilitates switching between main and support materials during the extrusion process in order to successfully build a part with internal features and overhangs. Then, the green part was shown to have good dimensional accuracy with respect to its CAD model. Finally, the green part was freeze-dried, debinded and sintered to remove the support material and achieve a good high-density ceramic part.

1.3. THESIS OVERVIEW

The study described in this thesis employed an alumina paste (Al_2O_3) consisting of powder, water, binder, lubricant and other materials, which was used simultaneously with a methyl cellulose paste consisting mostly of water. The solids loading of the ceramic paste was 45-55 vol. %. Water was the primary liquid medium in both the main and support material pastes, with an organic binder content of only 2–4 vol. %. A multiple-ram extruder mechanism was used to extrude both the main and support materials. The green part obtained after FEF fabrication was freeze-dried; then, the main material's binder and support material were removed through a burnout process before sintering to obtain the final part.

In the following sections, the FEF multiple-extruder system will be described in detail, highlighting the major process parameters. In Section 2, the hardware of the newly developed FEF system is described, as well as its function and interactions with other

hardware components. Section 3 details the dynamic modeling of the extrusion process for the pastes of both part and support materials. The differences between using the part material in the extrusion process and the support material also will be compared. Section 3 describes the testing of the controller capable of tracking reference forces for extrusion-on-demand (EOD) of both the part and support materials. This controller facilitated switching between the two pastes while the part was being fabricated. Section 3 also describes the experimental tests conducted to show the capability and performance of the FEF process. Section 4 outlines the measurement of the dimensional accuracy of the green part in comparison with the CAD model, as well as the measurement of the shrinkage percentage in the sintered part. Finally, the conclusions of the study are given in Section 5.

2. EXPERIMENTAL SETUP

The experimental system for freeze-form extrusion fabrication (FEF) with multiple extruders consists of a motion subsystem, a real-time control subsystem, and extrusion devices. A picture of the overall system is shown in Figure 2.1.
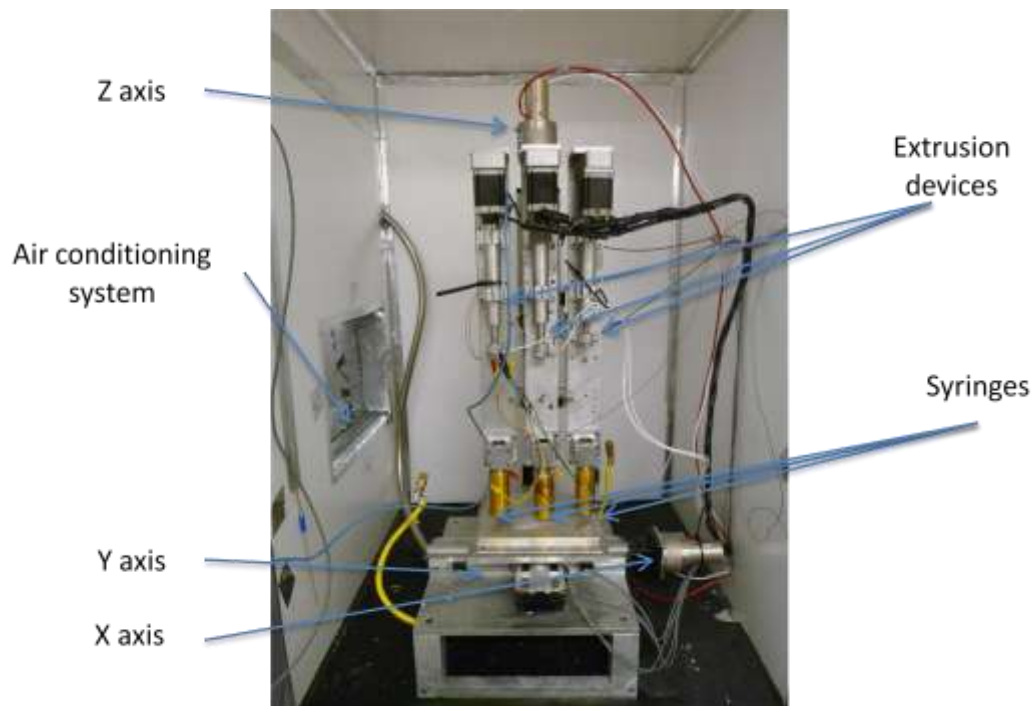
Figure 2.1. Experimental setup of the multiple-extruder FEF machine

2.1. POSITIONING SYSTEM

Three linear axes from Parker Hannifin (Daedal 404 XR) are driven by three stepper motors from Empire Magnetics. The X, Y and Z axes each have 254 mm of stroke. The gantry system motors have a stepping angle of 1.8^o. Each motor has a resolver that measures the angular position and feeds the signal to a resolver-to-digital encoder converter module (RDE). The RDE converts the resolver signal into an equivalent encoder feedback signal, thus allowing the resolution of each axis to be 2.5 μm per step. For each individual axis, the maximum velocity is 50 rev/s, or 250 mm/s in linear trajectories. The maximum motor acceleration is 50 rev/s^2, which provides a maximum linear axis acceleration of 250 mm/ s^2. The drives are used to amplify power from the motion control cards for the stepper motors. The Nu SX series drive from National Instruments is used. It has outputs for up to four stepper motors, as well as inputs for encoders and limit switches from four individual axes. The four outputs control the motions of three stepper motors for the X-Y-Z gantry system axes and one stepper motor for an extruder device. An NI MID series drive is used to regulate the two additional extrusion device motors. The drive has inputs from encoders and limit switches for up to two axes. The signals are processed by the amplifiers and sent through a 32-pin connector to two motion control cards. The drives are shown in Figure 2.2

NI PXI Real-time Controller

Motion cards

NI Nu SX drive

DAQ card

NI MID series drive

DAQ board

Figure 2.2. PXI NI N1011 chassis with real-time controller, two NI drives, two motion cards, one DAQ card, and one DAQ board

Based on previous research [16], the three gantry system axes exhibit a first-order response with a time constant of 3 ms. All of the three axes have the same dynamic characteristics, yielding identical dynamic models. The input is the command velocity (mm/s), and the output is the actual velocity (mm/s). The gain is 1, and the delay time is 5 ms.

2.2. REAL-TIME MOTION AND EXTRUSION CONTROL SYSTEM

A PXI National Instruments (NI) real-time system with LabVIEW is used for software development and graphical user interface. The real-time controller consists of a Pentium III 1.75 GHz Intel processor. The NI PXI 8176 real-time controller with 512 MB RAM is equipped with a 40 GB hard drive, two USB ports and two serial ports. The

chassis is a National instrument PXI N1011 with eight slots for PXI data acquisition cards (DAQ) and PXI motion cards. These cards are connected in the backplane of the chassis, allowing synchronous data processing to control the three stepper motors for the gantry system and the three stepper motors for the extrusion devices. Also, the real-time system comes with a multipurpose data acquisition card for discrete and analog I/O. Two NI PXI-7334 motion control cards are used to regulate the motors and read the RDE and encoder feedback signals. One card can control up to four individual axes, operated by either servo or stepper motors. The maximum pulse rate for the stepper motors is 4MHz, and the maximum encoder feedback rate is 20 MHz for each axis.

The NI PXI-6025 E multifunction data acquisition card is used for data input and output. It has two 24-bit counter timers, two 12-bit analog outputs, 32 digital I/O lines, and 16 analog input lines that can be used as single or double-ended inputs. The maximum sampling rate is 200 KS/s, with a minimum input operation range of -0.05 to 0.05 V to a maximum range of -10 to 10V.

2.3. EXTRUSION DEVICES

Multiple extrusion devices were used for the deposition of high solids loading ceramic pastes. Three extrusion devices, each having a resolution of 2846 steps/mm or 72882 steps/mm if using micro-stepping and a maximum velocity of 4 mm/s, were coupled directly to the Z-axis. The lead screw had 20 cm of linear travel. Three 50 cm^3 syringes contained the paste material for extrusion. A removable 580 μm diameter nozzle was used for depositing the material. By adjusting the commanded stepper motor speed,

the material deposition rate and the pressure on the syringe for extrusion by the ram can be controlled. A picture of the extrusion devices is shown in Figure 2.3.
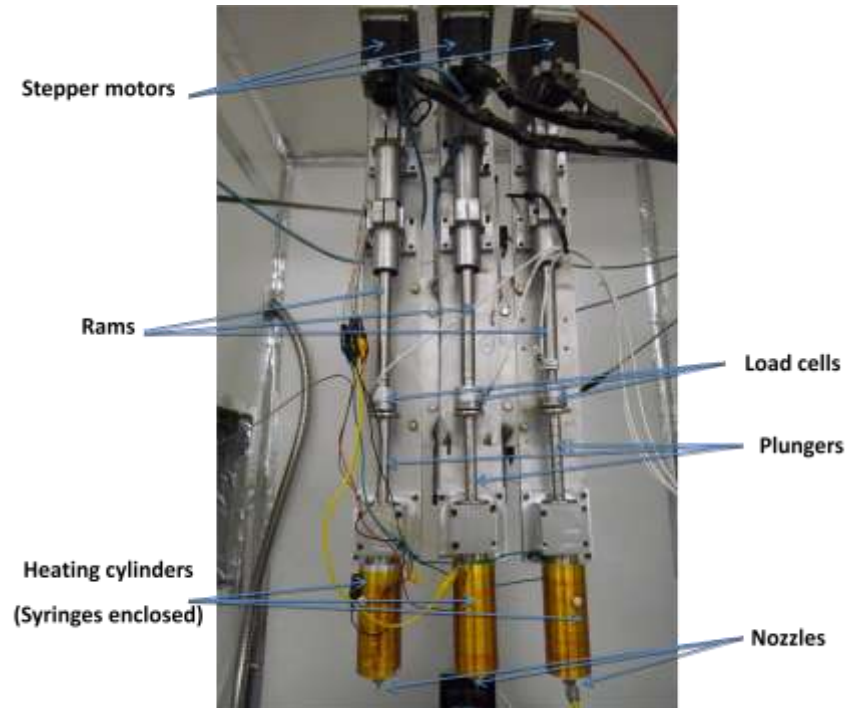
Figure 2.3. Three extrusion devices each consisting of a stepper motor, a ram, a load cell, a plunger, a syringe enclosed in a heating cylinder, and a nozzle

Three LC-301 load cells from Omega Engineering were fixed to three extruder rams for extrusion force feedback. The load cell measures the ram force while the ram is applying pressure to the ceramic slurry. A differential voltage (0 – 20 mV) is output by the load cell corresponding to an extruded force in the range of 0 to 2250 N. This output signal is increased by a factor of 483 through an amplifier that sends a discrete signal to the PXI DAQ card, therefore increasing the resolution of the load cell for force feedback. The load cell with a linearity of 0.1% yields an output within ± 4.45 N of the actual force.

2.4. STRUCTURAL COMPONENTS

The air conditioning system shown in Figure 2.4 was added to the freezer box in order to maintain the work environment at sub-zero temperatures. The syringes were covered by heating cylinders to prevent the paste from freezing before exiting the nozzle during part fabrication. Two temperature controllers from Omega Engineering (C132 and CN54) were used to control the temperature both inside the box and in the heating cylinders. Usually, the temperature inside the box was set to -10 °C, and the temperature for the heating cylinders was set to 20 °C (5 °C nozzles temperature).
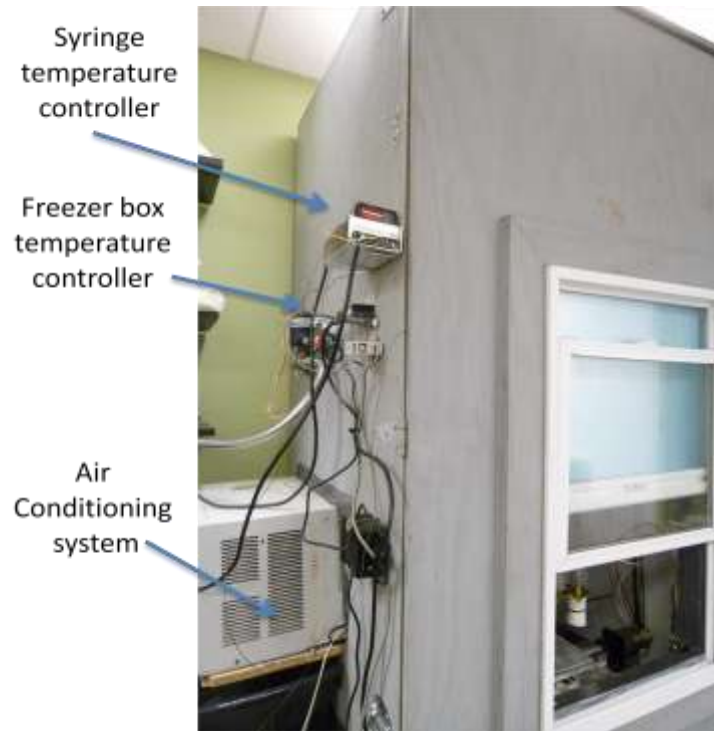
Figure 2.4. Air conditioning system and temperature controllers for freezer box and syringes

3. MODELING AND CONTROL OF PASTE EXTRUSION

3.1. MODELING OF PASTE EXTRUSION DYNAMICS

The extrusion of two different aqueous pastes, alumina and methyl cellulose, was modeled by running multiple extrusions to find out the parameters of a first-order system in the form of transfer functions, which were used to create the model. The model was used to test the system's response to a predefined input signal (ram command velocity) and the output (extrusion force). Analyzing the error involved identifying the difference between simulated and experimental data, and pinpointing which parameters yielded the error in the simulation.

3.1.1. Alumina Paste. The first-order model was used to characterize the extrusion based on results from previous studies [16-17]. Experimental tests were conducted, and the results were compared with simulations to verify the mathematical model and to obtain the unknown parameters. The paste composition per batch was 390 g of alumina prepared with 100 ml of distilled H_2O, 3.0 g of methyl cellulose, and 3.06 g of Darvan C.

A set of experiments was conducted to determine the relationship between extrusion force and ram velocity. These experiments are plotted in Figure 3.1. The ram velocities were 0.1, 0.2, 0.3 , 0.5 , 0.7 and 1 mm/s.
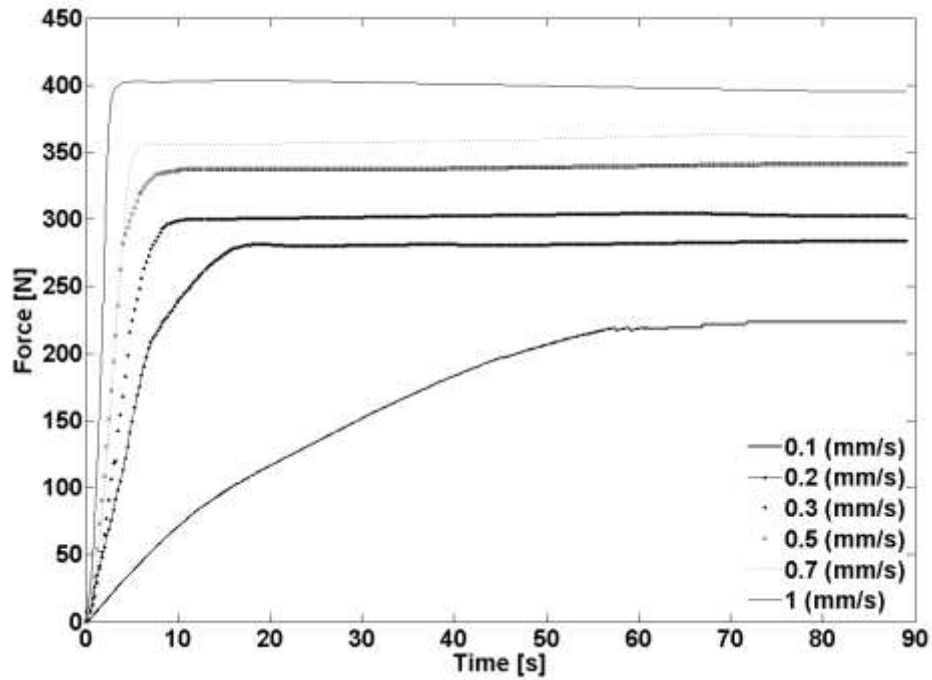
Figure 3.1. Alumina paste extrusion force dynamics for several ram velocity inputs

A first-order model was used to model the transfer function between extrusion force and ram velocity. The transfer function is given by

$$\frac{F(s)}{V(s)} = \frac{K}{\tau s + 1}$$

(1)

where s is the Laplace operator, F is the extrusion force, V is the ram velocity, K is the extrusion process gain and τ is the extrusion process time constant.

The time constant for a first-order is calculated with the following equation

$$\tau = 2.2 T_r$$

(2)

where T_r is the rise time (time taken from 10% to 90% of steady-state force) .

The gain is

$$K = \frac{F_{ss}}{V} \tag{3}$$

where F_{ss} is the steady-state force.

Table 3.1 shows the parameters calculated based on the data collected from the experiments shown in Figure 3.1.

Table 3.1. Time constant, steady-state force, and gain for alumina paste extrusion at different ram velocity inputs

Velocity (mm/s)	T (s)	F_{ss} (N)	K (N/mm/s)
0.1	22.15	216.88	2168.8
0.2	7.20	280.10	1400.5
0.3	4.43	301.47	1004.9
0.5	3.20	340.27	680.54
0.7	1.76	363.21	518.87
1	1.39	405.25	405.25

Based on the data collected in Table 3.1, the time constant decreases when a higher input velocity is applied to the ram. Comparing the time constant of 22.15 s for the velocity of 0.1 mm/s and the time constant of 1.39 s for the velocity of 1 mm/s, there is one order of magnitude difference in time constant.

The data from Table 3.1 was used to calculate the response of a first-order

system using Equation (1), which is digitized to the following difference equation:

$$f(i) = f(i-1) + \Delta t[-\frac{1}{\tau}f(i-1) + \frac{K}{\tau}v(i-1)] \qquad (4)$$

where f is the extrusion force and v is the ram velocity. Figure 3.2 compares the

simulation and experimental results. It shows that a first-order model is a good

approximation of aluminum paste extrusion dynamics.
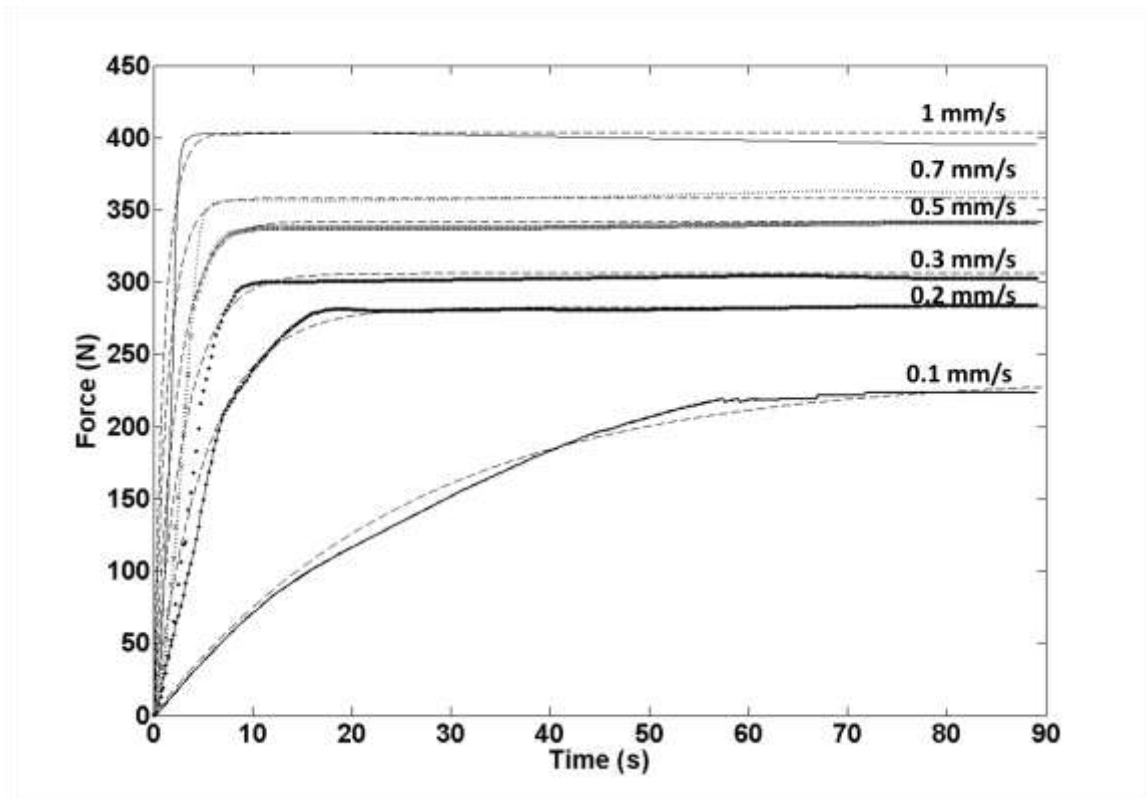
Figure 3.2. Comparison of simulation and experimental results based on gain and time constant for alumina paste extrusion from Table 3.1
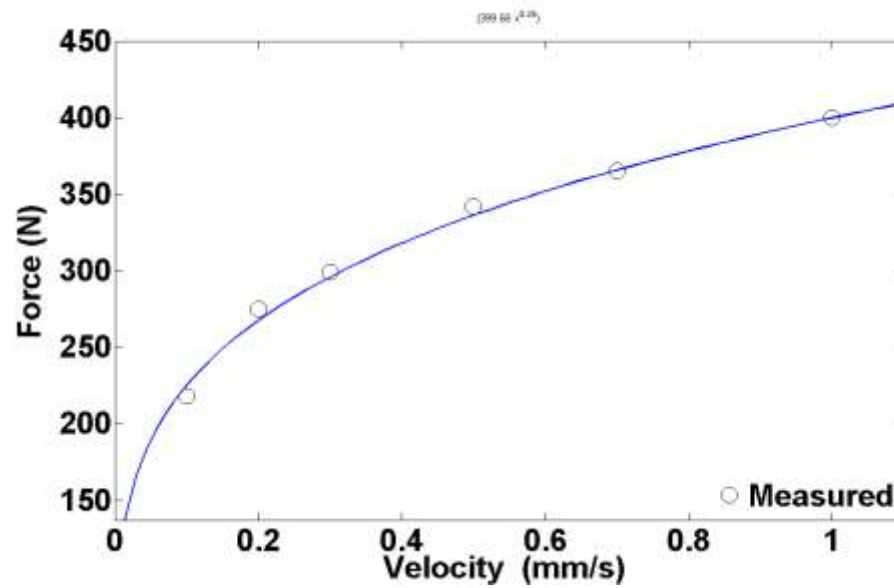
Figure 3.3. Relationship between steady-state force and ram velocity for alumina paste

From the values in Table 3.1, the relationship between the steady-state extrusion force vs. ram velocity is shown in Figures 3.3. The curve in Figure 3.3 shows a non-linear relationship between the steady-state force output vs. ram velocity input, where the data collected was fit into a power law to represent the nonlinear relation with a solid line. This is due to a nonlinear relation between paste viscosity and shear rate in a non-Newtonian fluid that can be described by the Herschel –Bulkley model (H-B) [25].

The power law in Figure 3.3 is given by

$$F_{ss} = 399.65v^{0.25} \tag{5}$$

where F_{ss} is the steady-state extrusion force and v is the ram velocity. The fitting of data by this equation was calculated with a correlation coefficient of 0.994.
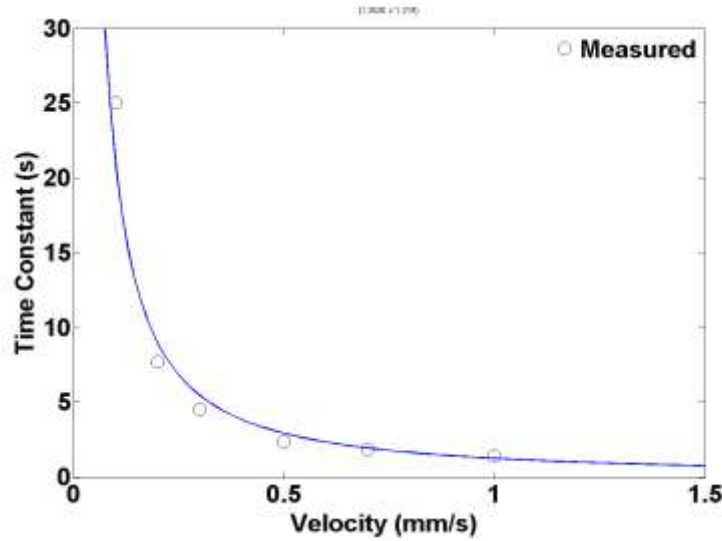
Figure 3.4. Relationship between time constant and ram velocity for alumina paste extrusion

Figure 3.4 shows the relation between time constant and ram velocity for alumina paste extrusion based on the measured values from Table 3.1. The data from Figure 3.4 was fit into a power law whose equation is

$$\tau = 1.159 \, v^{-1.249} \tag{6}$$

where τ is the time constant and v is the ram velocity.

The correlation coefficient is 0.97 indicating a very good approximation. Figure 3.4 shows that the time constant decreases when the ram velocity increases. This phenomenon was described in the dynamic modeling of non-linear paste behavior by Li et al. [21]. This model considered some volume of air within the syringe and derived a linearized dynamic extrusion force model, which shows that the time constant decreases when the extrusion force or ram velocity increases.

Based on above results, a linearized first-order model was used to represent the dynamic behavior of the paste. The time constant and gain were calculated in the operating range of forces in which the steady-state extrusion force vs. ram velocity exhibited a linear relation in order to apply a feedback force controller for extrusion on demand.

In order to verify the values obtained from Figure 3.1 and apply a robust feed-back force controller, a linearized first-order model was obtained. The time constant and system gain parameters were calculated in the digital domain using the Recursive Least Square method (RLS) [17] within the operational range of forces. A first-order dynamic model describing the paste extrusion force of the process in the digital domain is

$$G(z) = \frac{F(z)}{V(z)} = \frac{b}{z+a} = \frac{K(1+a)}{z+a} \qquad (7)$$

where z is the forward shift operator, F is the extrusion force (N), V is the command velocity (mm/s), and K is the unknown model gain (N/mm/s).

The time constant and gain, respectively, are

$$\tau = -\frac{T}{ln(-a)} \qquad (8)$$

$$K = \frac{b}{1+a} \qquad (9)$$

where T is the sampling time, and τ is the time constant.

The difference form of Equation (7) is

$$f(i) = af(i-1) + K[1-a]v(i-1) = \eta(i-1)\varphi(i-1) \tag{10}$$

where i is the current iteration, and the vector of unknown parameters is

$$\eta = [a \quad (i-1)a] = [a \quad b] \tag{11}$$

The vector of regression variables is

$$\varphi(i) = [f(i-1) \quad v(i-1)]^T \tag{12}$$

The parameters are estimated by computing them recursively using the following equations. The recursive covariance matrix calculated based on its previous value is

$$P(i) = [I - q(i)\varphi^T(i)]P(i-1) \tag{13}$$

where

$$q(i) = P(i-1)\varphi(i)[I + \varphi^T(i)P(i-1)\varphi(i)]^{-1} \tag{14}$$

The estimated parameter vector which contains a and b values is

$$\eta(i) = \eta(i-1) + q(i)[y(i) - \varphi^T(i)\eta(i-1)] \tag{15}$$

The matrix P is the covariance matrix. The initial covariance matrix was selected to be a 2x2 diagonal matrix with values equal to the number of samples from the experimental data. The matrix I was a 2x2 identity matrix. The input and output are shown in Figure 3.5.
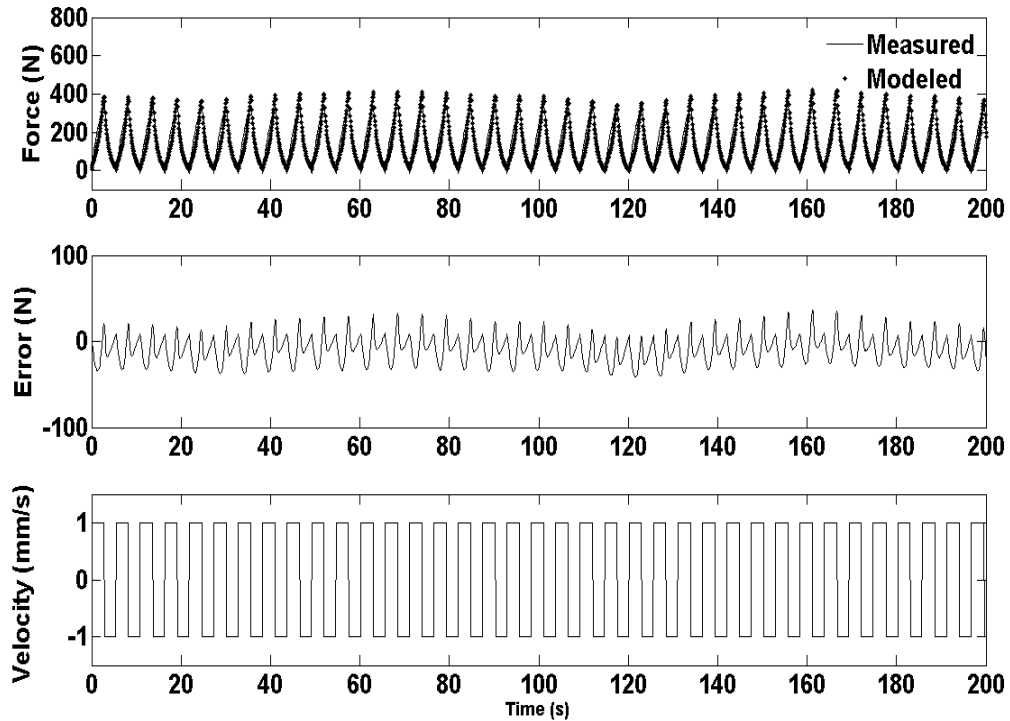
Figure 3.5. Comparison of modeled data to the measurements obtained with a step reference input for alumina paste

The system was tested with a series of step inputs over 200 seconds and several cycles to obtain the output force during the extrusion process. The velocity was varied from 1 mm/s to - 1 mm/s with a square signal input with a frequency of 0.167 Hz and a 50% cycle time.

A relatively small percentage of error (maximum of 15% of the absolute

magnitude of force) was recorded during the comparison of the experimental results with

respect to the estimated model. An input of -1 mm/s was provided to stop the extrusion of

the paste and to decrease the time constant. The model parameters were estimated using

Equations (14–16). The model's estimated first-order dynamic parameters were obtained

and compared to the previous experimental data from Table 3.1. The parameters,

calculated with a sampling rate of $T = 0.1$ s, were $a = -0.931$ and $b = 27.86$. The time

constant was $\tau = 1.40$ s, and the gain is $K = 403.76$ N/mm/s, both of which were almost the

same as the values in Table 3.1 ($\tau = 1.39$ s and $K = 405.25$ N/mm/s).

The average error between the modeled and measured forces varied between +/-

30 N (15% with respect to the absolute amplitude). Hence, there was good agreement

when using a first-order process approximation to represent the system's dynamics.

3.1.2. Methyl Cellulose Paste. Two different materials were tested to find

the adequate support material for the FEF extrusion process. The first support material

tested was carbon black. The decision to use this material was based on previous research

by Lewis et al. [12] on AM processes with ceramic material using sacrificial materials.

The composition of the experimental carbon black paste was 48 vol. % carbon black ink,

4 vol. % methyl cellulose binder and 48 vol. % water. The carbon black paste did not

work well due to its viscosity inconsistency. The carbon black reacted differently at room

temperature with less humidity (30% humidity) than inside the freezer box at sub-zero

temperatures with higher humidity (80% humidity). The humidity inside the freezer box

made the carbon black paste smudged after the deposition of extrudate lines. This

phenomenon could be explained by the fact that the water content in carbon black powder

is increased by 4% when there is an increase of 10 % in humidity in the environment

[24]. The carbon black paste viscosity was affected by the moisture inside the freezer

with the increase of water content by almost 20 vol. % (due to increase of humidity from

30% to 80%) from its original composition. The reason that carbon black was not suitable

for the FEF process but was successful in the Direct Ink Writing (DIW) [22] was due to

the fact the DIW process was performed in room temperatures (without change of

humidity) while the FEF process was performed sub-zero temperatures (with large

change of humidity). Moreover, the part in the DIW process was fabricated in a pool of

oil to prevent change in the viscosities of the main and support materials. Due to the

incompatibility of carbon black paste for the FEF process, an alternative sacrificial

material was used. Methyl cellulose was chosen due to its good rheological properties at

sub-zero temperatures. The composition of methyl cellulose paste used in our study was

10 vol. % methyl cellulose binder and 90 vol. % water content. The first set of

experimental tests involved applying constant ram velocities to the plunger in the syringe

containing the support material paste.

The command velocity of the ram was kept constant at 0.1 mm/s for 160 seconds,

and extrusion force data was collected at a rate of 10 Hz. The extrusion force vs. ram

velocity plot is shown in Figure 3.6. Four tests were conducted with a 580 μm diameter

nozzle. During the tests, a steady state of 170 N was reached, suggesting that the applied

force and ram velocity are related. A first-order empirical model was used for paste

extrusion simulation.

The data was averaged and fit to a first-order model using Equations (1), and Equation (4) was used to simulate a first-order response:
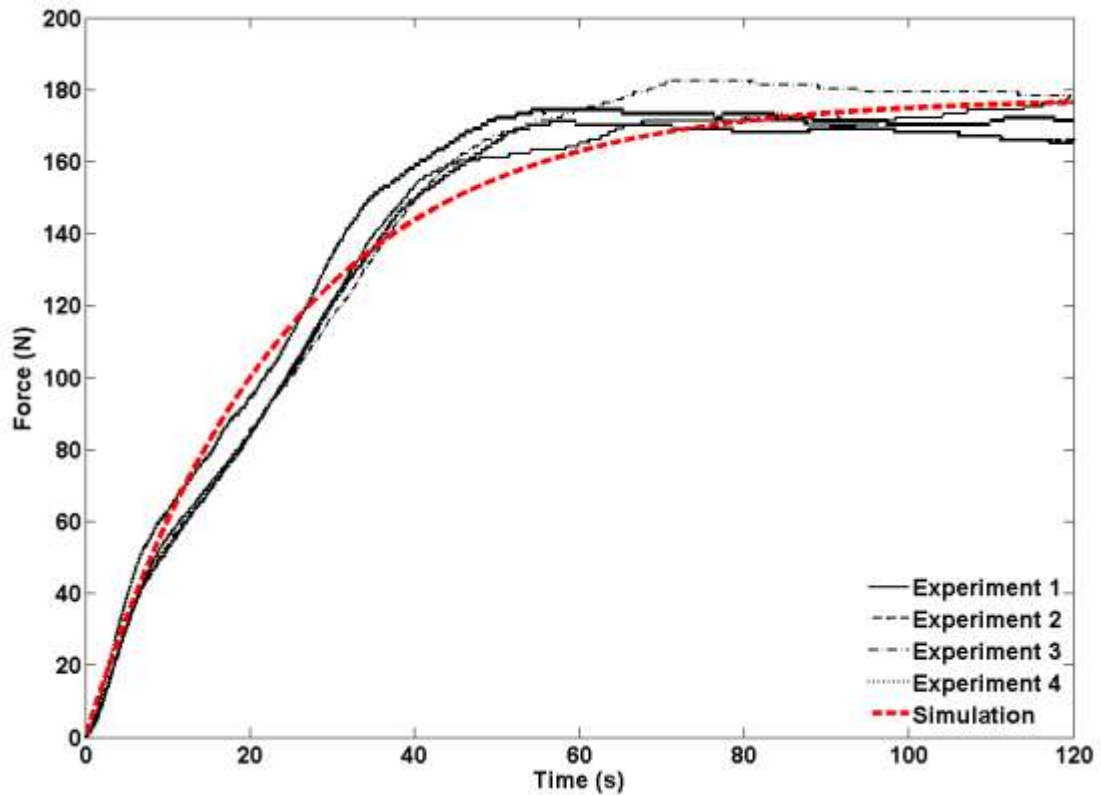
Figure 3.6. Extrusion force response for methyl cellulose paste with ram velocity of 0.1 mm/s as the input

The second set of experimental tests involved varying the velocity input until steady-state force extrusion was reached. The experiments are plotted in Figure 3.7. The ram velocities were 0.1, 0.2 , 0.3 , 0.5 , 0.7 and 1 mm/s. Figure 3.7 shows a variation of steady-state force constants at different input velocities.
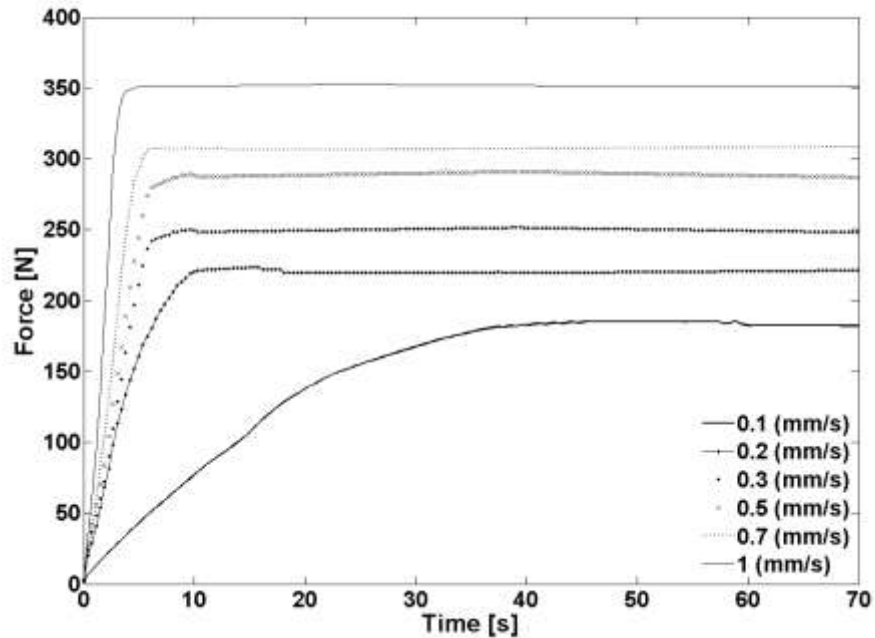
Figure 3.7. Methyl cellulose paste force dynamics given a constant ram velocity input

The curves exhibited a first-order response between steady-state force as the output, and ram velocity as the input. Based on these data, the time constant and steady-state force were calculated graphically using Equations (1-3). Table 3.2 shows the parameters calculated based on Figure 3.7.

Table 3.2. Time constant, steady-state force, and gain for methyl cellulose paste at different ram velocity inputs

Velocity (mm/s)	T (s)	F_{ss} (N)	K (N/mm/s)
0.1	18.55	176.23	1762.3
0.2	6.10	222.14	1110.7
0.3	3.44	248.37	827.9
0.5	2.90	296.24	592.48
0.7	1.75	320.54	457.14
1	1.36	353.20	353.20

Using the data from Table 3.2 and Equation (4), different curves were simulated for different velocities. The curves are shown in Figure 3.8.
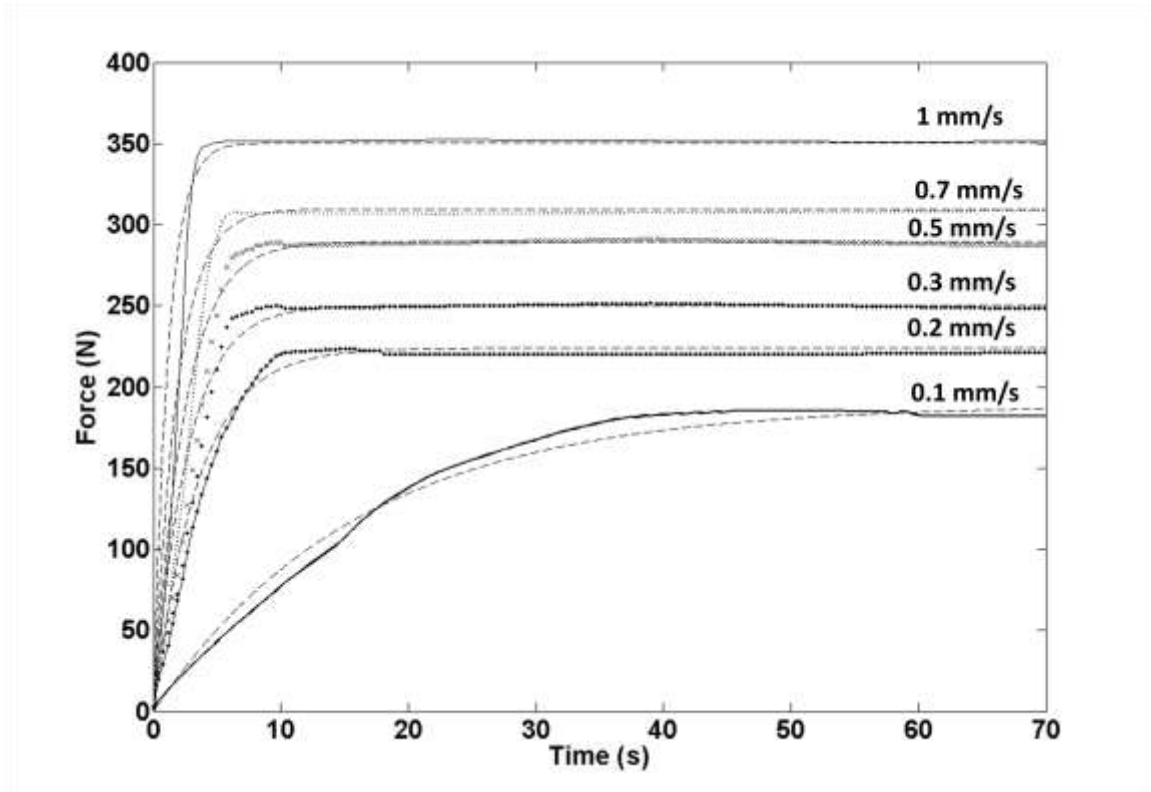
Figure 3.8. Simulation and comparison of different curves based on gain and time constant for methyl cellulose from Table 3.2

Figure 3.7 shows the simulation of a first-order response of force with respect to a constant ram velocity. It could be seen from Table 3.2 that if the input ram velocity was high, the time constant decreased and the output steady-state force increased. There is a good approximation of the simulated to experimental curves. The curve shown in Figure 3.9 was obtained by plotting the steady-state forces for every input command ram velocity.
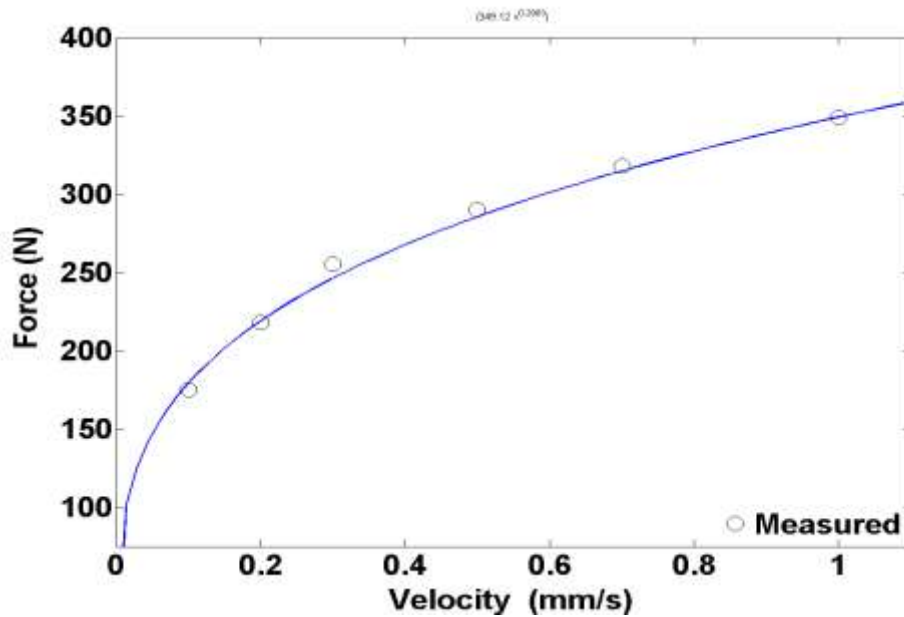
Figure 3.9. Relationship between steady-state force and ram velocity for methyl cellulose paste

Figure 3.9 showed the non-linear relation between steady-state force and command velocity for the methyl cellulose paste, which was similar to the extrusion of alumina paste. The paste exhibited a non-Newtonian fluid behavior. The data was fit into a power law shown in Figure 3.9 with a solid curve. The power law is

$$F_{ss} = 349.12v^{0.29} \tag{16}$$

where F_{ss} is the steady state force and v is the ram velocity. The equation had a correlation coefficient of 0.99, showing a very good approximation.

The relationship of time constant vs. ram velocity is shown in Figure 3.10. The data was fit into the following power law

$$\tau = 1.2734 \, v^{-1.087} \tag{17}$$

where τ is the time constant and v is the ram velocity. The correlation coefficient was 0.96 showing a very good approximation. The time constant decreases with the increase in the ram velocity. This non-linear relation is similar to the alumina paste and can be explained using the model described by Li et al. [21].
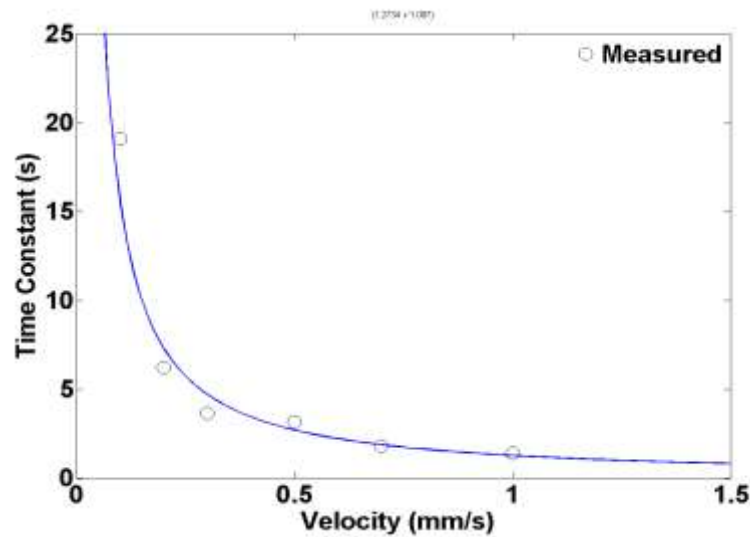
Figure 3.10. Relationship between time constant and ram velocity for methyl cellulose paste

In order to verify the data obtained in Table 3.2 and design a robust linear model-based force-feedback controller, an approximation of the non-linear system to a linearized first-order empirical model was obtained in the force ranges. The open-loop time constant and system gain parameters were calculated based on the RLS method

using Equations (10-15). The input and output are shown in Figure 3.11. The system was

tested with a series of step inputs over 200 seconds and several cycles to obtain the output

force during the extrusion process. The velocity was varied from 1 mm/s to -1 mm/s with

a square signal input with a frequency of 0.167 Hz and a 50% cycle.
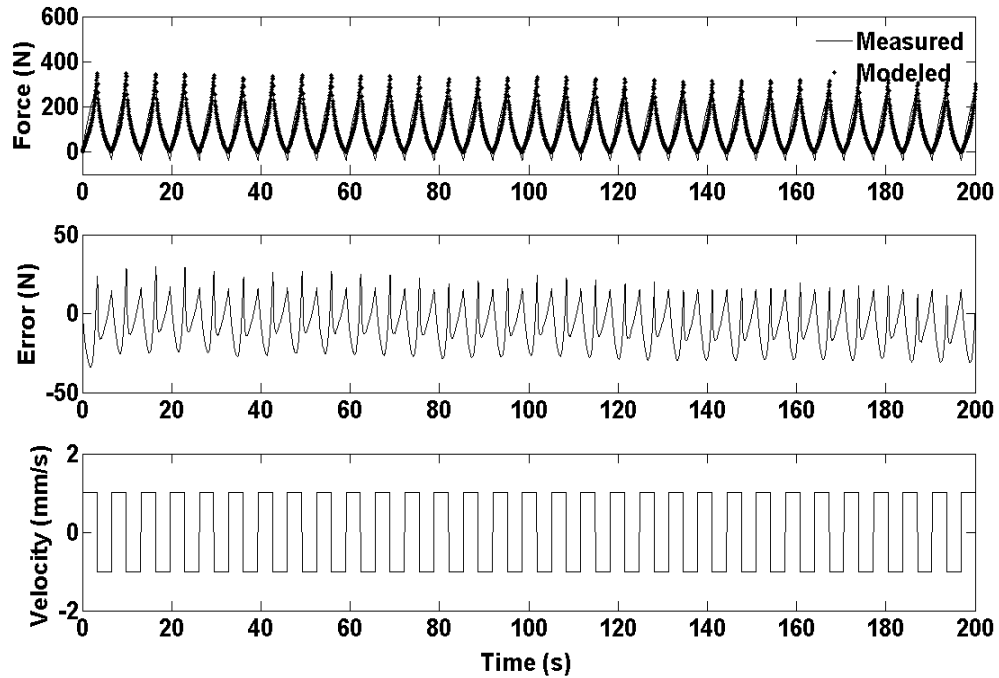
Figure 3.11. Comparison of modeled data to the measurement obtained with a step
reference input for methyl cellulose

The parameters, calculated with the sampling rate of T=0.1 s are a= -0.929 and

b= 24.67. The time constant τ was 1.371 s, and the gain K was 347.45 N/mm/s. These

parameters were similar to those previously calculated and shown in Table 3.2 which

were a time constant of 1.36 s and a gain of 353.20 N/mm/s for an input of 1mm/s.

The average error between the modeled and measured forces was +/- 25 N, which was 14% of the output amplitude. Hence, there was a good agreement for using a linearized first-order dynamic model to represent the open-loop system.

The input of 1 mm/s was used to start the methyl cellulose paste extrusion as fast as possible in order to decrease the time constant in the open-loop system. Likewise, the input of -1 mm/s was used to stop the extrusion of methyl cellulose paste as fast as possible in order to decrease the time constant in the open-loop system.

3.2. CONTROLLER DESIGN AND IMPLEMENTATION

Due to certain effects of extrusion, such as the release of air bubbles, the breakdown of agglomerates, and the change in paste properties as a result of liquid phase migration, the extrusion force is difficult to control in open loop [16-18]. A linear model-based General Tracking Controller (GTC) was implemented to regulate the extrusion force in a close-loop manner. The schematic diagram of a GTC controller is shown in Figure 3.12.
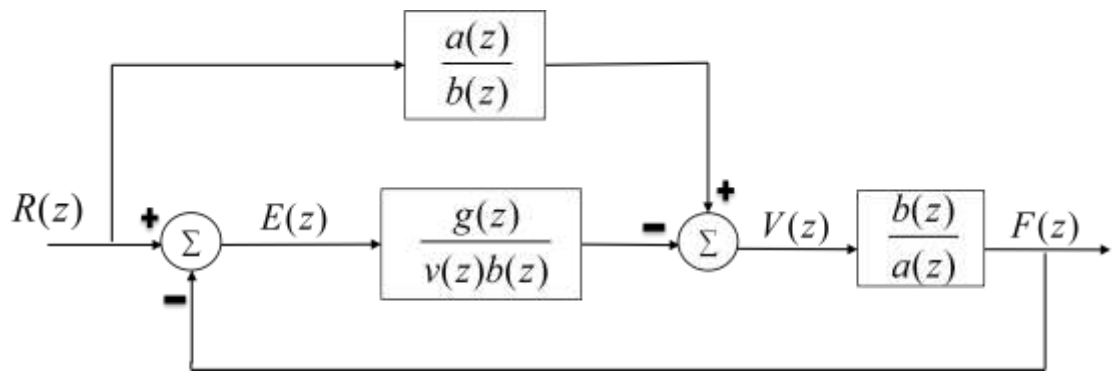
Figure 3.12. Block diagram of GTC

A control algorithm was designed to allow extrusion on demand during the FEF

process in order to extrude the paste at a constant rate and to coordinate the start of

extrusion with the gantry motion. This algorithm uses the GTC to reject constant

disturbances with desired error dynamics. The control signal is related to error and

reference signals by

$$b(z)v(z)V(z) = v(z)a(z)R(z) + g(z)E(z) \tag{18}$$

where $v(z)a(z)$ is the disturbance-generating polynomial, and $v(z) = z - 1$ is the reference

disturbance for a step reference input. Because $b(z)V(z)=a(z)F(z)$ we have

$$v(z)a(z)F(z) = v(z)a(z)R(z) + g(z)E(z) \tag{19}$$

$E(z)$ is the error defined as

$$E(z) = R(z) - F(z) \tag{20}$$

then

$$[v(z)a(z) - g(z)]E(z) = 0 \tag{21}$$

where $R(z)$ is the reference ram extrusion force, $F(z)$ is the measurement from the load cell, $a(z)$ is the denominator of the open-loop transfer function, and $g(z)$ is a first-order polynomial, i.e.,

$$g(z) = g_1 z - g_0 \tag{22}$$

where g_1 and g_0 are determined by the desired closed-loop error dynamics, i.e.,

$$g_1 = -1 + a - \alpha_1 \tag{23}$$

$$g_0 = -a - \alpha_0 \tag{24}$$

where α_1 is

$$\alpha_1 = -e^{(-T/\tau_1)} \tag{25}$$

and α_0 is

$$\alpha_0 = -e^{(-T/\tau_2)} \tag{26}$$

The closed-loop characteristic equation is

$$\alpha(z) = z^2 + \alpha_1 z + \alpha_0 \tag{27}$$

Equation (23) can be rewritten as

$$[z^2 + (1 - a - g_1)z + (-a - g_0)]E(z) = 0 \tag{28}$$

For the system to have a response similar to a first-order system, one pole should be of a much smaller magnitude than the other pole. This was achieved by making the second pole at least one order of magnitude smaller than the dominant pole. The settling time was decreased without causing system instability using the dominant pole.

The difference equation for the controller is

$$U(i) = U(i-1) + \frac{1}{b}[R(i+1) + (a-1)R(i) - a\,R(i-1) - g_1\,E(i) - g_0 E(i-1)] \qquad (29)$$

The error equation is

$$E(i) = R(i) - F(i) \qquad (30)$$

3.2.1. General Tracking Controller for Extrusion of Alumina Paste. Using Equations (23-26) and the model parameters calculated with the RLS method, the parameter g_1 was -1.07 and g_0 was 1.06. Equation (29) and (30) were implemented in LabVIEW RT software. To validate the tests, an input square signal was given with low and high limits of 100 N and 400 N, respectively, as shown in Figure 3.13.
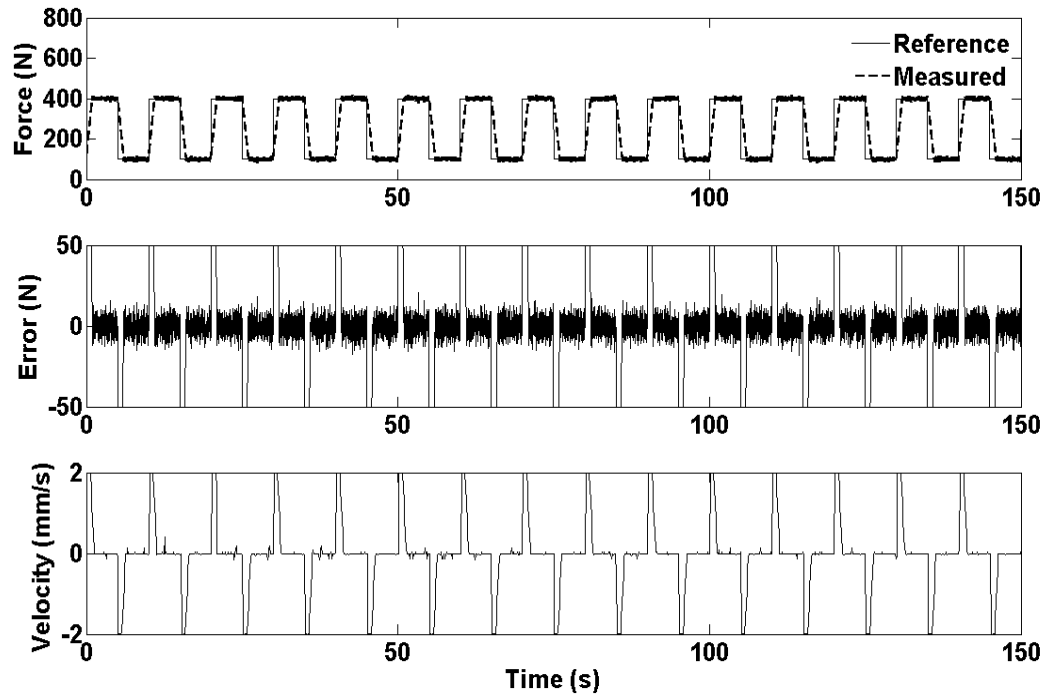
Figure 3.13. Response of the ram force controller for a reference force input for extrusion of alumina paste

Two over-damped poles were selected with the time constants $\tau_1 = 0.5$ s and $\tau_2 = 0.05$ s. Therefore, the time constant of the closed-loop system was determined by τ_1. The closed-loop constant was determined by the mechanical limitations of the machine. The maximum input velocity for the process in our FEF system was 2 mm/s, at which the maximum force of 550N provided by the stepper motor in the system was reached. The open-loop time constant for 2 mm/s for the system was calculated using Equation (6) and the time constant obtained was $\tau = 0.48$ s . The closed-loop time constant was chosen as 0.5 s, in order to have the quickest response of the system without overloading the motor. The reference force was set at 400N (slightly less than 550N for margin of safety) for extrusion of alumina paste. The force of 100 N was used to stop the extrusion based on

experimental test runs that will be explained later. The GTC controller tracked the

reference force with an error of +/-10 N, giving a good extrusion rate when depositing

material. By looking at the reference vs. measured force plot in Figure 3.14, the time

constant of the closed-loop system calculated from the rise time is approximately 0.5 s

using Equation (2). This time constant is reduced by 65% from 1.39 s in the open-loop

system for a 400N output force.
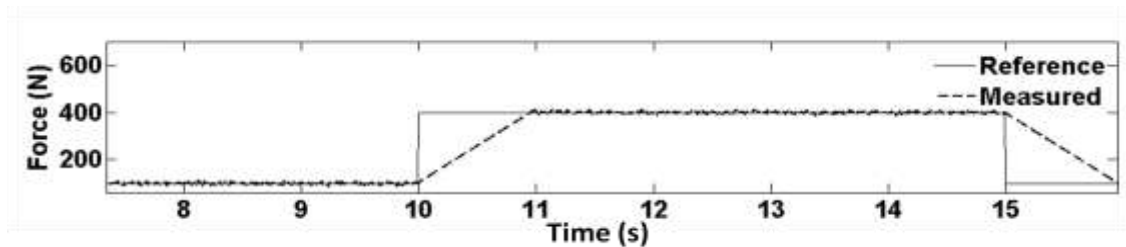
Figure 3.14. Reference vs. measured force using GTC controller with a rise time of 1s
for alumina

The input signal was set to +/- 2mm/s to get a faster time response of the system

without falling into instability. Higher velocities would cause the stepper motor to skip

and not able to track the reference force properly.

A series of tests was conducted to find a relationship between the extrudate

velocity and the reference force in the close-loop system. Table 3.3 was generated by

varying the reference force from 150 N to 200N, then to 300N, and finally to 400 N. The

tip of the nozzle was positioned along the Z directions 50 mm above the gantry X-Y

table. The velocity was calculated by measuring the time it took for the paste to reach the

X-Y table from the moment it was extruded from the tip. A stopwatch with a resolution

of 0.1 s was used for this time measurement. Six test runs per reference force were

conducted and averaged to verify its repeatability. The different tests per reference force

show similar values verifying the advantage of using a GTC controller. Table 3.3 was

made to obtain a relation between the extrudate velocity versus the reference force.

Table 3.3. Relationship between reference extrusion force and extrudate velocity for alumina paste

Test run	Distance (mm)	Force (N)	Test 1 (s)	Test 2 (s)	Test 3 (s)	Test 4 (s)	Test 5 (s)	Test 6 (s)	Mean extrudate speed (mm/s)
1	50	150	80.1	82.3	85.4	84.3	82.1	82.8	0.6
2	50	200	42.1	40.1	44.2	43.2	42.1	42.3	1.18
3	50	300	20.1	21.2	22.0	21.8	20.9	21.2	2.35
4	50	400	12.3	13.1	14.2	13.5	12.9	13.2	3.78
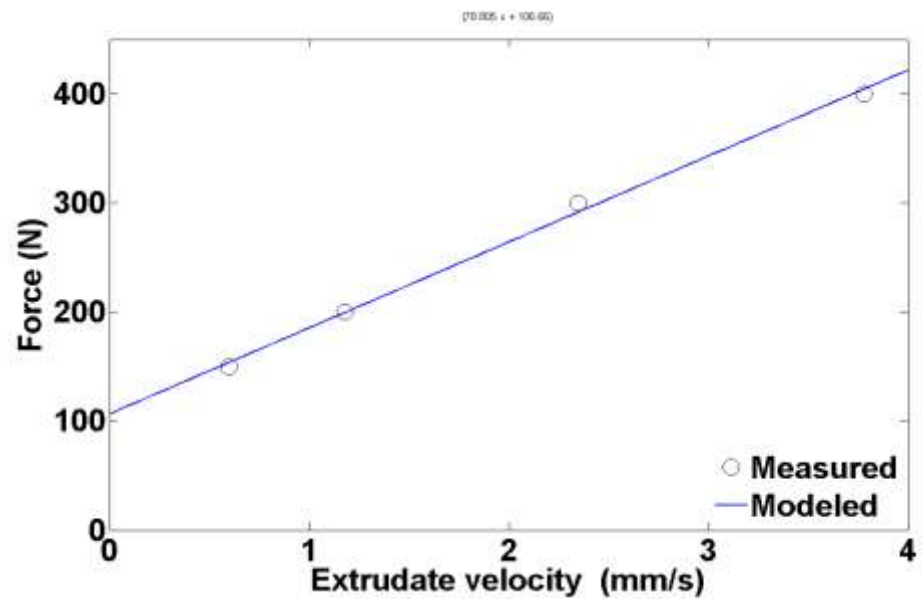
Figure 3.15. Reference force extrusion vs. extrudate velocity for alumina paste

A linear regression between the extrusion force and extrudate velocity was applied. The result is shown in Figure 3.15. The correlation coefficient is 0.997, which is a very good approximation. The equation relating the extrusion force with the extrudate velocity is

$$F_{ss} = 78.805V_{ex} + 106.66 \qquad (31)$$

where F_{ss} is in N and V_{ex} is in mm/s. The linear approximation indicated that the feedback force controller within the operating ranges made the system to have a linear dynamic response. Thus, the relationship between steady-state force and extrudate velocity can be regarded as linear. The y intercept shows that when the extrudate velocity is zero, the steady- state force is 106.6 N. Hence, the minimum force required to extrude paste from the nozzle tip is ~100 N. If the extrusion force is less than this threshold, extrusion will cease because the applied ram force is not enough to overcome the shear stress.

Rapidly increasing the force will help control the paste extrusion during extrusion on demand. A low reference force will prevent the alumina paste from leaving the nozzle when it is desired to cease extrusion. A high reference force will maintain a constant extrusion rate to keep the deposition consistent and avoid disturbances such as the release of air bubbles. For the stepper motors used in our system, the ram extrusion can only apply a force of up to 550 N; once this limit is reached, the motor will skip in order to reduce the torque being applied. Due to this limitation, a force limit of 400N was used and the closed-loop time constant achieved was 0.5 sec.

The time constant of the closed-loop control system was 0.5s with the GTC controller, compared to the open-loop system with a time constant of 1.39 s. Thus the time constant of the system has been reduced by 65% using closed-loop control.

The error of the closed-loop system was +/-10 N when reaching the reference force, as shown in Figure 3.16. This error was considerably small, thus providing a consistent extrusion rate during part fabrication. The closed-loop controller was saturated with an input velocity of +/- 2 mm/s (Figure 3.13); above this velocity, the controller's instability makes it incapable of tracking the reference force properly.

3.2.2. General Tracking Controller for Extrusion of Methyl Cellulose Paste

Following the same procedure used for the alumina paste, g_1 and g_0 in Equations (23-26) were calculated. Given the model parameters calculated with the RLS method for methyl cellulose paste, the value of g_1 was -1.11 and g_0 was 1.06. The values of g_1 and g_0 were implemented in Equation (29) in LabVIEW RT software. To validate the tests, an input square signal was given with low and high limits of 50 N and 350 N, respectively. The reference value of 350N was chosen to start the paste extrusion. The reference value of 50 N was used to stop the extrusion based on experimental test runs to be explained later. The GTC system had an error of when reaching the settling time in +/-10 N, giving a consistent extrusion rate when depositing methyl cellulose material. The GTC test result is shown in Figure 3.16.
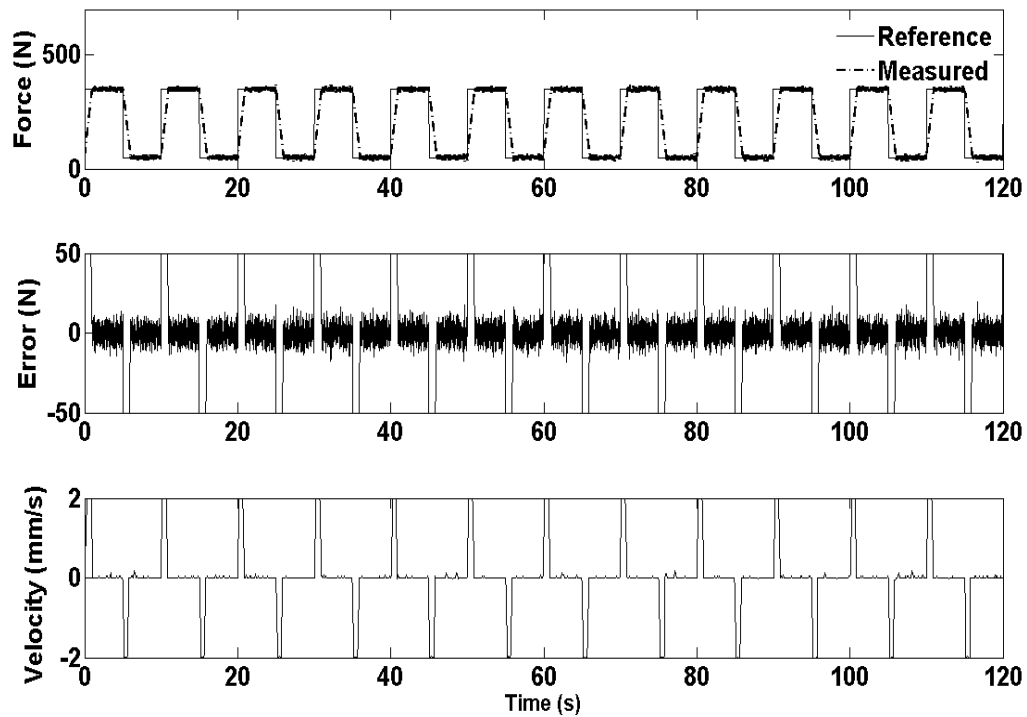
Figure 3.16. Response of the ram force for a reference force input for extruding methyl cellulose paste

The closed-loop time constant was calculated based on the open-loop time constant for a ram velocity of 2 mm/s. Based on Equation (17) the time constant calculated was $\tau = 0.59$ s, thus the time constant of 0.5 s was again chosen in order to be the same as the time constant used in the closed-loop control of alumina paste extrusion. With this time constant the rise time was approximately 1 s, and thus the time constant of the open-loop system (1.36 s) was reduced to 0.5 s (65% reduction) for the steady-state extrusion force of 350 N in the closed-loop system. By looking at the plot of measured force vs. time, the rise time of the closed-loop system was approximately 1s (Figure 3.17) as expected.
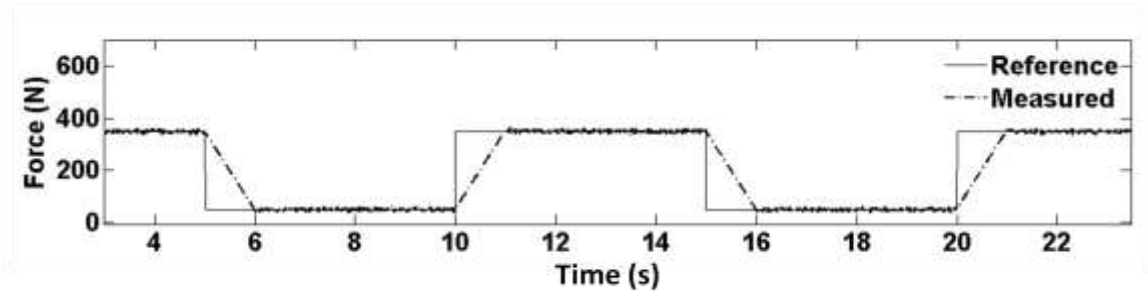
Figure 3.17. Reference vs. measured force using GTC controller with a rise time of 1s
for methyl cellulose

Similar to alumina paste extrusion the closed loop-system and a time constant of

0.5 s. The input signal was set to +/- 2mm/s to get the fastest possible response of the

system without falling into instability. Higher velocities would cause the system to

become unstable due to overloading the extrusion device. This made the stepper motor

skip and not able to track the reference force properly. The error of the controller was +/-

10 N when reaching the reference force (Figure 3.16). This error was considerably small,

thus providing a consistent extrusion rate during part fabrication.

Similar to the procedure used for the alumina paste, a series of tests was

conducted to find the relationship between the velocity of methyl cellulose extrudate and

the reference force. Table 3.4 was created by varying the reference force from 100 N to

150, then to 250, 300, and finally 350 N. The tip of the nozzle was positioned along the Z

direction 50 mm above the gantry X-Y table. The velocity was calculated by measuring

the time it took for the paste to reach the X-Y table from the moment it was extruded

from the tip. A stopwatch with a precision of 0.1 s was used for this measurement.

The experiment was run six times per reference force to see its repeatability

giving consistent experimental results proving the capability of the GTC controller.

Table 3.4. Relationship between reference extrusion force and extrudate velocity for
methyl cellulose paste

Test run	Distance (mm)	Force (N)	Test 1 (s)	Test 2 (s)	Test 3 (s)	Test 4 (s)	Test 5 (s)	Test 6 (s)	Mean extrudate speed (mm/s)
1	50	100	70.8	71.2	71.2	70.5	69.8	70.7	0.7
2	50	250	35.3	33	34.5	35.8	35.1	34.7	1.44
3	50	300	18.5	17.5	18.0	18.5	18.0	18.1	2.76
4	50	350	12.5	13.0	12.7	13.1	13.3	12.9	3.87

A curve fit was applied to find the relationship between the extrusion force and

extrudate velocity, as shown in Figure 3.18. Figure 3.18 revealed a linear relationship

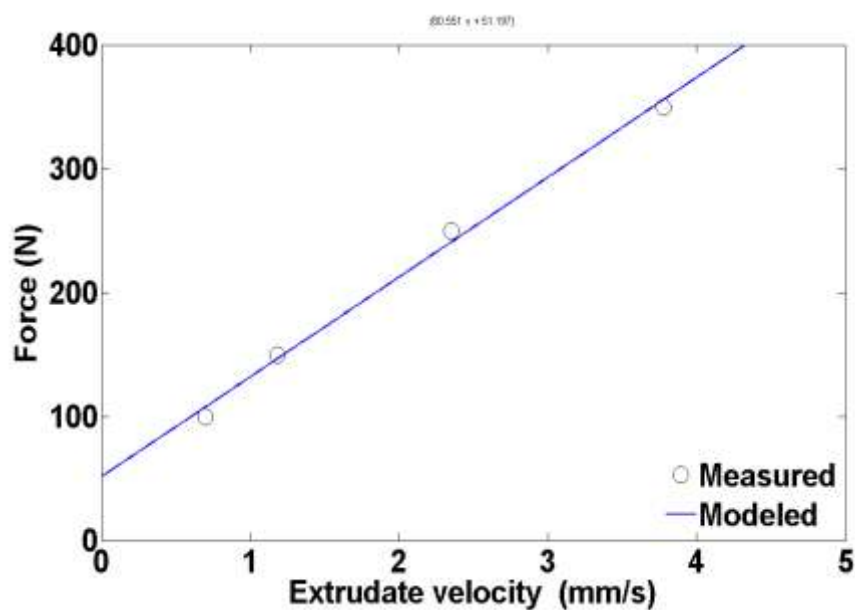between the extrusion force and extrudate velocity.

Figure 3.18. Steady-state force vs. extrudate velocity for methyl cellulose

The equation relating the extrusion force with the extrudate velocity can be given as

$$F_{ss} = 80.551 V_{ex} + 51.197 \qquad (32)$$

where F_{ss} is in N and V_{ex} is in mm/s.

The correlation coefficient was 0.996, which was a very good approximation. Similar to alumina paste, when using the GTC controller the relation between extrudate velocity and steady-state force was linear in the operating range of 50-350N. This means that the controller will help overcome non-linear behavior in the paste compared to a non-linear relation between extrusion ram velocity and steady state force in the open-loop system.

The y intercept shows that when the extrudate velocity became zero, the steady state force became 51.2 N, indicating that the minimum force required to extrude paste from the nozzle tip is ~50 N. If the extrusion force is less than this threshold, the extrusion will stop because the shear rate is not enough to initiate extrusion. Rapidly increasing the force will help control the paste extrusion with a faster time response than in the open-loop system. The low reference force will prevent the methyl cellulose paste from leaving the nozzle, and the high reference input will maintain a constant extrusion rate to keep the deposition consistent. The ram force was set to 350N because the ram force had to be approximately 50 N less than the reference force in alumina in order to mach the extrudate velocity with alumina paste extrusion, as can be seen in Figures 3.15 and 3.18.

3.3. EXTRUSION PARAMETERS AND MOTION COORDINATION

The quality of part fabricated by the FEF process will be affected by parameters including the stand-off distance, starting and stopping of the extrusion process, table speed, and freezing time. This section discusses the determination of effective parameters for the FEF process with use of support material. In all of the experiments, the diameter of the needle nozzle was 580 μm.

3.3.1. Stand-off Distance. Using the maximum extrusion force in the FEF process, which was 400N for alumina and 350 N for methyl cellulose, the extrudate diameter was, respectively, 780 μm and 760 μm, for a freezer temperature of -10 °C. Experiments were conducted to measure the extrudate width by varying the stand-off distance. The range of stand-off distances varied from 700 to 400 μm in decrements of 100 μm. The path was a serpentine trajectory of 4 lines, the table speed was 8 mm/s, and the extrusion force was 400 N for alumina and 350 N for methyl cellulose. The lines were measured using a caliper with a resolution of 10 μm. Five straight lines were deposited in order to see the repeatability of the process in giving a consistent extrudate width for each stand-off distance. It could be seen that the shorter the stand-off distance, the wider the extrudate. This was due to the fact that the extrudate diameter of the paste coming out of the nozzle had a diameter larger than the stand-off distance. This caused the extrudate lines to flatten out and have an almost rectangular cross-sectional area instead of a circular cross-sectional area. The results for alumina paste extrusion are shown in Table 3.5.

Table 3.5. Relationship between stand-off distance and extrudate width for alumina

Test run	Stand-off distance (μm)	Line 1 Width (mm)	Line 2 Width (mm)	Line 3 Width (mm)	Line 4 Width (mm)	Line 5 Width (mm)	Mean Width (mm)
1	400	1.23	1.25	1.22	1.21	1.23	1.22
2	500	1.15	1.12	1.10	1.11	1.11	1.11
3	600	1.0	0.98	0.96	0.95	0.94	0.96
4	700	0.80	0.79	0.81	0.80	0.76	0.79

The same experiment was repeated using methyl cellulose. Again, the range of stand-off distances varied from 700 to 400 μm in decrements of 100 μm. The path was a serpentine trajectory of 4 lines, the table speed was 8 mm/s, and the extrusion force was set to 350 N. The lines were measured using a caliper with a resolution of 10 μm. The results are shown in Table 3.6. The consistency of the process was also tested when extruding 5 lines per stand-off distance. The extrudate width had a very small variation from 20 to 10 μm with respect to the mean width varying from 800 μm to 1200 μm

Table 3.6. Relationship between stand-off distance and extrudate width for methyl cellulose

Test run	Stand-off distance (μm)	Line 1 Width (mm)	Line 2 Width (mm)	Line 3 Width (mm)	Line 4 Width (mm)	Line 5 Width (mm)	Mean Width (mm)
1	400	1.21	1.20	1.22	1.21	1.20	1.20
2	500	1.10	1.11	1.08	1.10	1.08	1.09
3	600	0.99	0.98	0.95	0.97	0.98	0.98
4	700	0.80	0.82	0.81	0.80	0.80	0.80

Comparing the results of alumina and methyl cellulose, the extrudate widths differed only between 10 and 30 μm with the same stand-off distances. This difference is negligible; thus, the same stand-off distance was used in extruding alumina and methyl cellulose in building a part with both part and support materials.

Three stand-off distances of 400 μm, 500 um and 600 μm were used, and two alumina blocks of 10 x 5 x 30 mm^3 were fabricated for each of these three stand-off distances with a table speed of 8 mm/s. The results of these fabrications under an extrusion force of 500 N are shown in Figure 3.19.
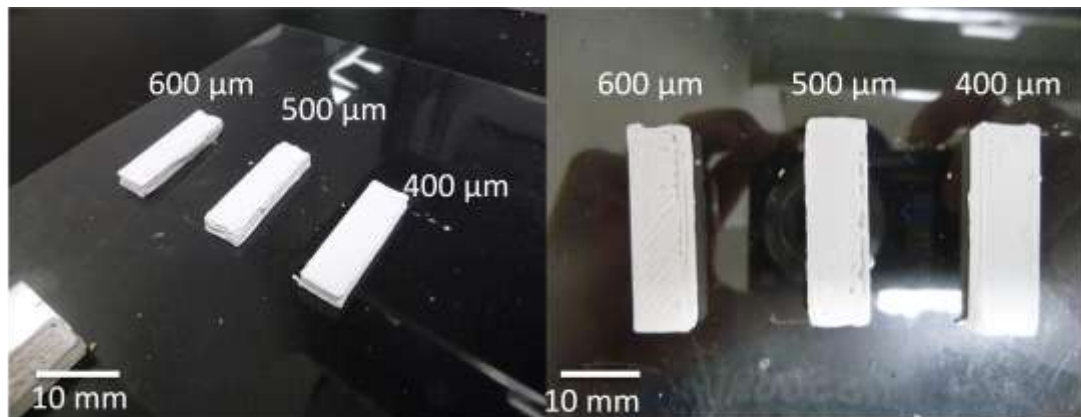

Figure 3.19. Stand-off distances varying from 600 to 400 μm of alumina blocks
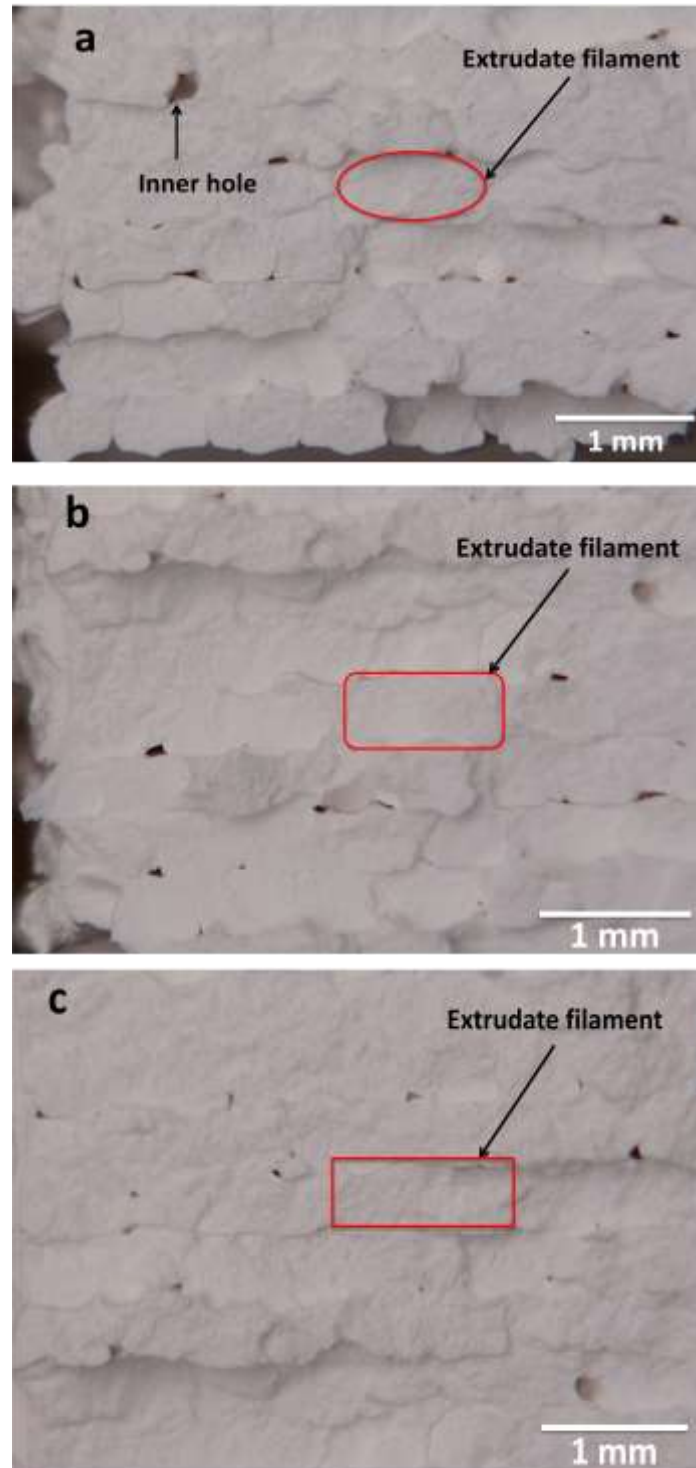
Figure 3.20. Cross sections of extrudate blocks with the stand-off distance of (a) 600 μm, (b) 500 μm, and (c) 400 μm

The cross sections from the blocks with different stand-off distances are shown in Figure 3.20. The block with 600 µm stand-off distance (see Figure 3.20a) shows extrudate lines with rounder edges and some inner holes among extrudate lines. The block with 500 µm stand-off distance (see Figure 3.20b) shows extrudate lines with sharper edges and fewer and smaller inner holes among extrudate lines. Figure 3.20b also exhibits a good solid infill in the extrudate cross-sectional area. The block with 400 µm stand-off distance (see Figure 3. 20c) also shows extrudate lines with sharper edges and fewer smaller inner holes among extrudate lines. Therefore, good results were obtained using 400 µm and 500 µm stand-off distances. Larger stand-off distances (above 600 µm) will result in poor deposition of the material, and smaller stand-off distances (below 400 µm) will result in paste accumulation at the tip of the nozzle. In further experiments the stand-off distance of 500 µm was used when extruding both alumina and methyl cellulose pastes in building a part with both part and support materials.

3.3.2. Table Speed. The table speed is crucial to good paste deposition. For this purpose, six test runs were conducted in which the table speed was varied from 4 mm/s, which was the extrudate velocity in the extrusion operating range for alumina and methyl cellulose, to 14 mm/s in increments of 2 mm/s. The pictures in Figure 3.21 for both alumina and methyl cellulose show the results of extrusion using an extrusion force of 400N and 350N, respectively. The stand-off distance of 500 µm was used` for both alumina and methyl cellulose material pastes.
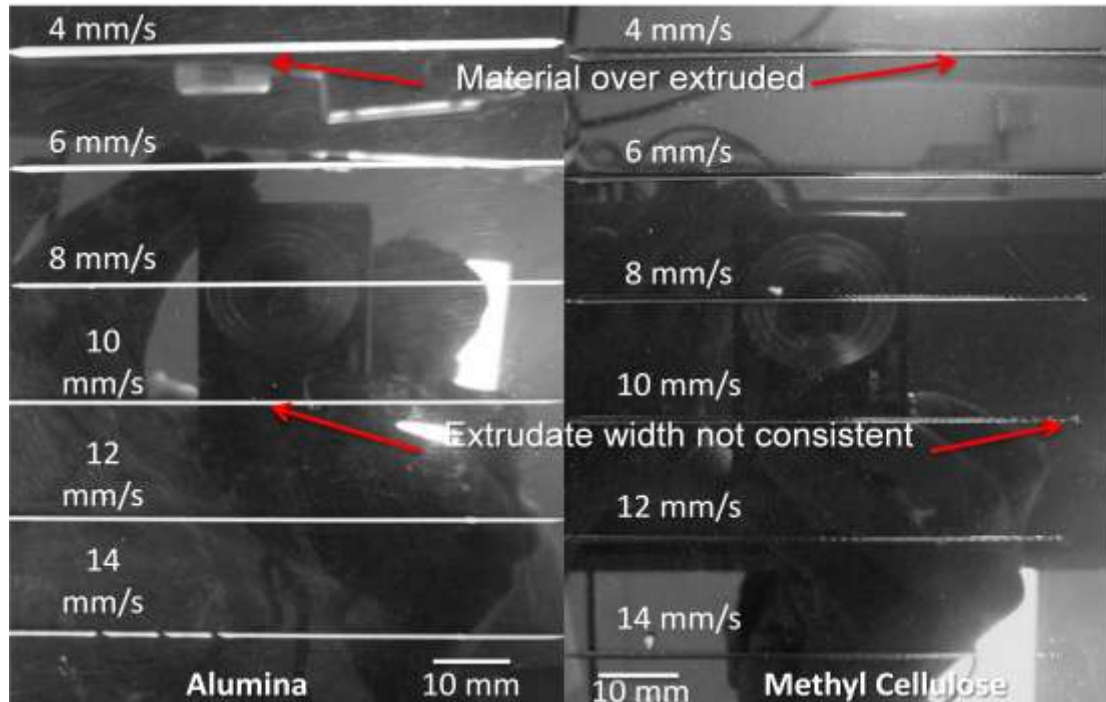
Fig 3.21. Different table speeds for alumina (left) at 400 N extrusion force and for methyl cellulose (right) at 350 N using 500 μm stand-off distance

When the table speed was 8 mm/s the deposition for both alumina and methyl cellulose pastes had relatively uniform width compared with other table speeds. At velocities higher than 10 mm/s, irregular width for the extrudate lines and inconsistent deposition was observed. Such a deposition could lead to gaps between lines during the rastering process, which could result in poor-quality parts, as shown in Figures 3.21 and 3.22. The build time and surface quality of the parts also depend upon the table speed. It has been reported previously that maintaining the extrusion speed at table speed yields a good deposition of filaments [16]. However, maintaining the table speed at the extrusion speed could result in an over-extrusion of material surrounding the needle tip as shown in the schematic in Figure 3.22.
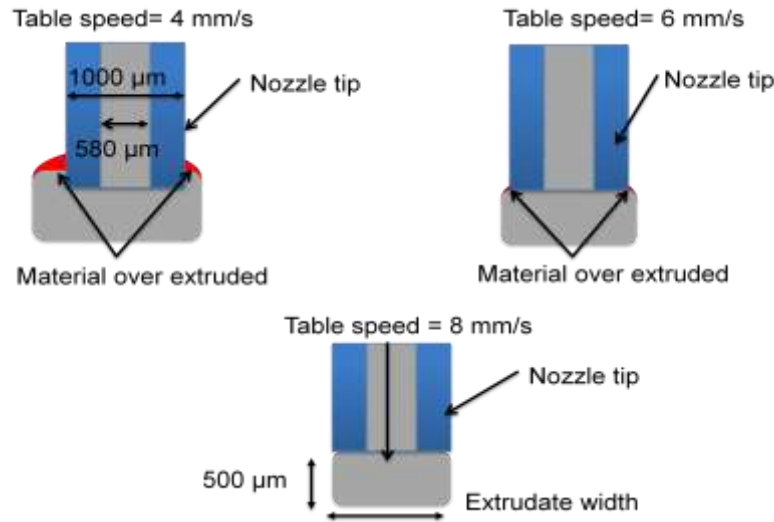
Fig 3.22. Illustration of different problems at different table speeds during paste extrusion. The extrudate speed was 4 mm/s and the stand-off distance was 500 μm, which was 86% of nozzle diameter

The equation based on conservation of paste flow is:

$$V_T = \frac{V_{ex}\pi D^2}{4wh}$$

(33)

where V_T is the Table speed, V_{ex} is the extrudate speed, D is the extrudate diameter (780 μm), w is the extrudate width and h is the stand-off distance (extrudate height). From Equation (33) it can be calculated that when the table speed is 4 mm/s the extrudate width is 1.91 mm, which is much larger than the outer diameter of the nozzle; thus, there is an over-extrusion of paste material and the width of the extruded paste line is not very uniform. When the table speed is 6 mm/s the line width of the extruded paste is 1.21 mm, which is slightly larger than the nozzle's outer diameter. When the table speed is 8 mm/s, the extruded paste line width is 0.95 mm, which is slightly smaller than the nozzle's outer diameter. This explains why the extrudate line was most uniform when the table speed was 8 mm/s, which was the desired table speed.

3.3.3. Advanced Times for Starting and Stopping Paste Extrusion. It takes a

certain amount of time for the paste extrusion control system to reach the desired high

force level to begin extruding paste; likewise, it takes some time to reach the desired low

force level to stop the extrusion process, as shown in Figures 3.14 and 3.17. To determine

these advance times needed to start and stop the paste extrusion, experiments were

conducted during the extrusion of alumina and methyl cellulose pastes. These

experiments consisted of extruding straight lines to achieve a constant distance of 80 mm

starting from one desired point and ending at another desired point. The extrusion had to

be set to start before the start point of trajectory and to stop before reaching the end point

of trajectory. This method was used because there was a time delay between the step

reference force input and the actual force output when using the GTC. The results of the

early force extrusion start and stop times for alumina and methyl cellulose can be seen in
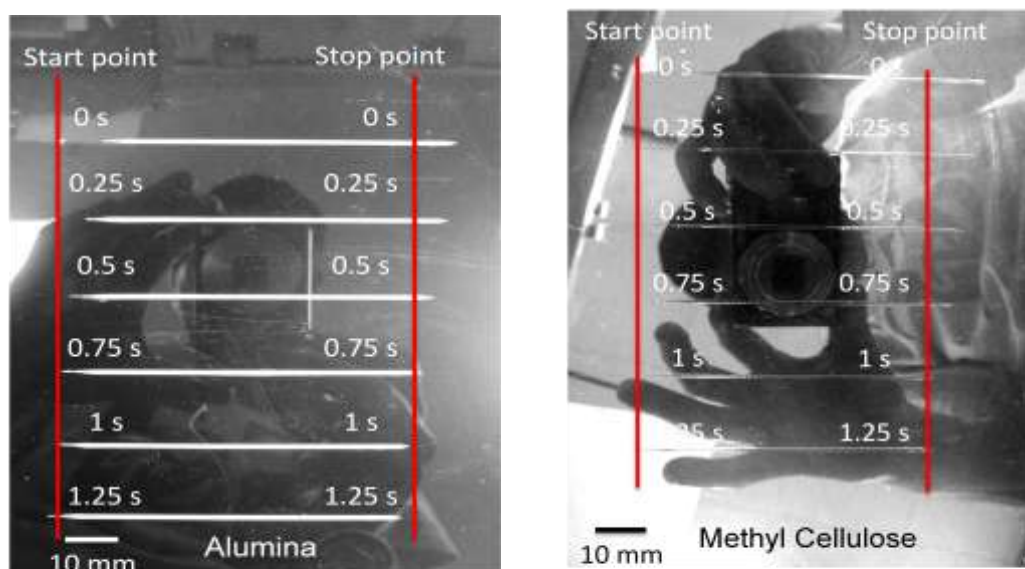
Figure 3.23.

Figure 3.23. Different advance start and stop times for of alumina (left) and methyl
cellulose (right)

Based on a comparison of the extrusion results of alumina and methyl cellulose pastes, starting and stopping paste extrusion without early start/stop commands could result in inaccurate deposition locations. This causes paste deposition to begin after the desired start point and to end after the desired stop point, which would affect rastering and contouring operations. Figure 3.23 shows the results of the start and stop tests for alumina and methyl cellulose. If the extrusion of the paste started at the time the needle tip reached the start point and stopped at the time the needle reached the stop point, there was an extrusion delay for the desired start and stop points within the trajectory. On the other hand, if there was a start extrusion command before reaching the desired start point and stop extrusion command before reaching the desired stop point, the extrudate line length could approach the desired start and stop points accurately.

The best results from this set of experiments were achieved in both alumina and methyl cellulose with an advance time of 1s before reaching the desired start point and an advance time of 1s before reaching the desired stop point. This advance time for paste extrusion was the same as the rise time in the closed-loop controller. Hence, regardless of the paste composition, whether alumina or methyl cellulose, the time response was the same when using a closed-loop controller whose time constant can be determined by the controller. The advance time of 1s was the input into the tool generation path software to fabricate the part.

3.3.4. Motion Coordination. The new FEF machine consisted of multiple extruders to fabricate 3D parts from multiple pastes. A commercially available software, along with Matlab, was used with LabVIEW to coordinate the motion of these extruders (during the deposition process) to switch between different materials. The process also

incorporated Extrusion-on-Demand (EOD) control. Experiments were conducted for the coordinated motion.

3.3.4.1. Tool path generation software. Skeinforge is an open source software program that we have used to generate the tool path for both alumina and methyl cellulose. An STL file of a CAD model is required to generate this path. The inputs of the Skeinforge software were parameters such as extrudate width, standoff distance, and table speed that were determined previously through experimentation. EOD was regulated using the early distance-based start method (8 mm for 8 mm/s table speed) and early distance-based stop method (8 mm for 8mm/s table speed).

3.3.4.2. Motion code for parts with support material. The first step was to calculate the distance between the nozzle tips between the extrusion devices, which was 99 mm along the y-axis, as shown in Figure 3.24.
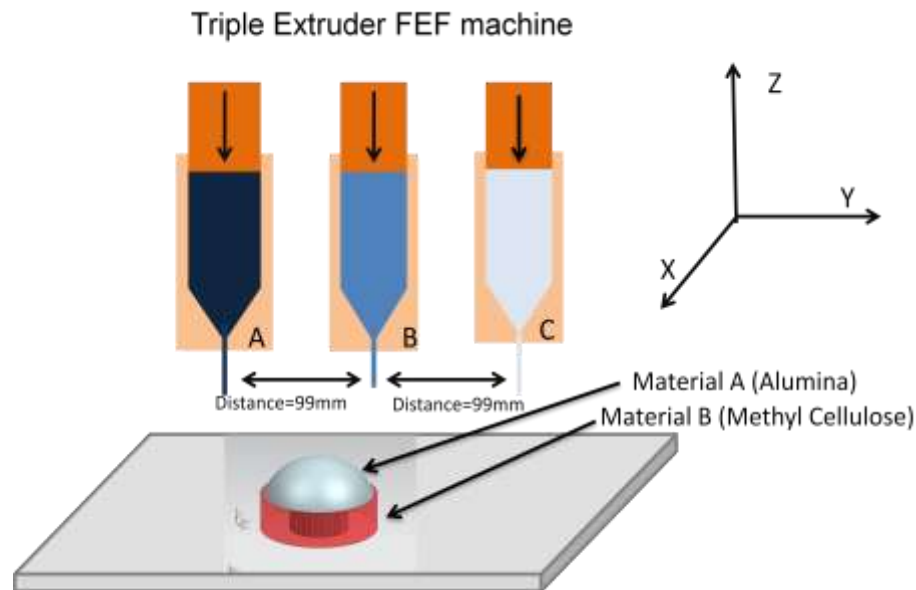

Fig 3.24. Schematic of the triple extruder machine

Skeinforge was used for path generation. It can require multiple STL files as input depending on how many materials a user wants to use to make one part (Figure 3.24). The output of the program is G-code. The multiple extruder system cannot interpret this machine code, so a converter script in C++ was written to translate from G-code to a code that the system could understand

To convert the G-code generated by Skeinforge into a code that LabVIEW could understand, the X-Y-Z coordinates were rearranged, as well as the M101 and M103 commands for starting and stopping of extrusion, respectively. A fourth column of start/stop commands was added to identify when the extrusion is to begin or end with the M101 and M103 commands from Skeinforge. For example, when extruding alumina, the extrusion flag will be 101 to start extrusion and 103 to stop extrusion. To extrude methyl cellulose, the start extrusion flag will be 201, and the stop code will be 203. If a third extruder is needed, the codes will be 301 and 303 to start and stop, respectively. The general conversion script from G-code to LabVIEW code was written in C++.

In order to combine the motion G-codes for the main and support materials, a Matlab script was used to link the main material code with the support material code based on the third column values, which represented the layer height. To extrude the first layer of the part, the code will first read the alumina paste coordinates to be extruded. After finishing the motion code for alumina, the motion code for the support material will run until reaching the end of the last point and that particular layer height. An example of the LabVIEW code is shown in Figure 3.25.

Figure 3.25. Conversion from G-code to LabVIEW code schematic

4. EXPERIMENTAL RESULTS

4.1. PART FABRICATION

Several parts were fabricated to demonstrate the capabilities of the developed FEF process. The surface quality was improved by adding a waiting time between layers in agreement with simulation studies [23] and by reducing the stand-off distance in every layer from 600 µm in early experiments to 500 µm. This was performed in order to improve the part's dimensional accuracy. The first experiments involved using a support material to make two parts with simple geometries. These two parts are shown in Figures 4.1 and 4.2, which also include the tool paths for the deposition of part material.
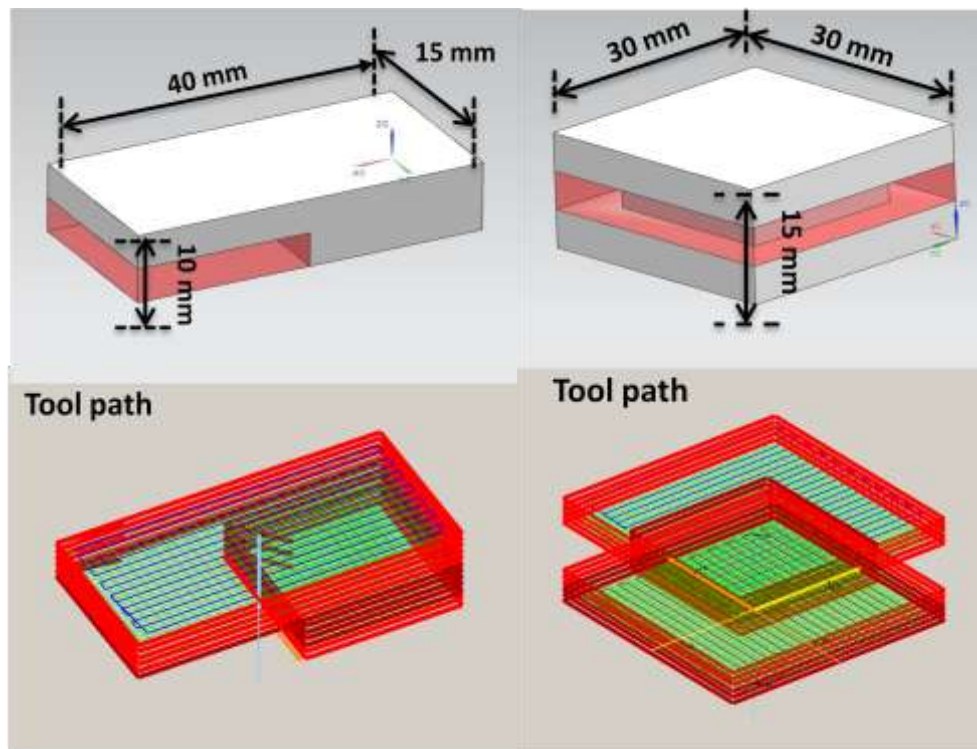
Figure 4.1. CAD models and tool paths of two different blocks
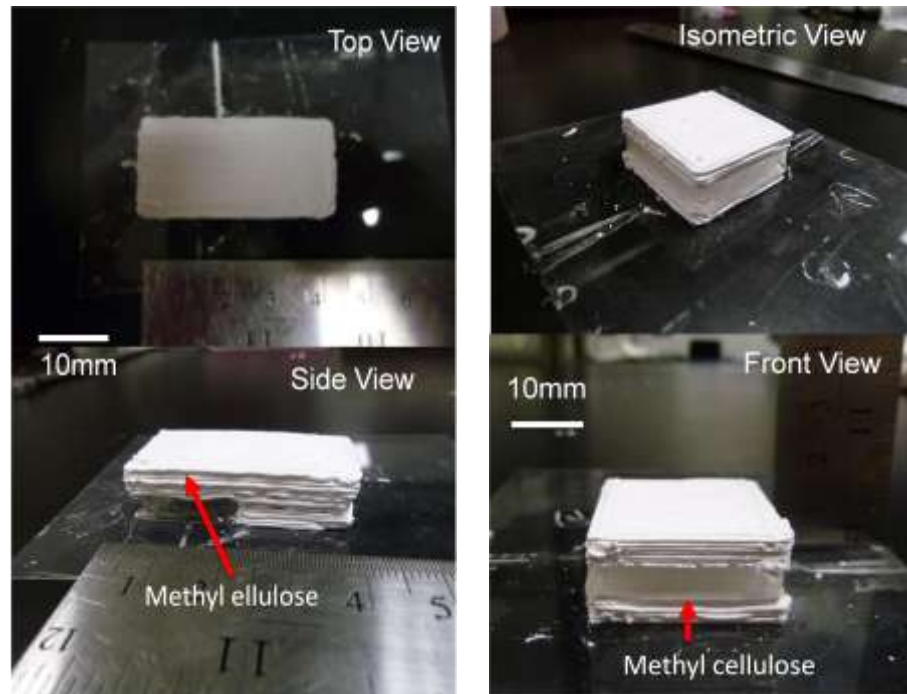
Figure 4.2. Extruded parts of two different blocks using FEF process with sacrificial materials

These first two experiments (Figure 4.2) were conducted using a stand-off distance of 600 μm since the process was tested in early stages. The surface finishing was not good due to the fact that the extrudate cross-section was circular-shaped and not rectangular-shaped. When building parts higher than 15 mm and using a stand-off distance of 500 μm, the waiting time between layers was not long enough for the new layer to be deposited. Beyond the 30th layer, the previous layer could not freeze completely and led to poor surface quality, as shown in Figure 4.3.

Figure 4.3. CAD models and extruded parts using FEF process with sacrificial materials without waiting time

The study by Li et al. [23] reported the simulated waiting times needed to freeze alumina paste at different layer heights. Their results sho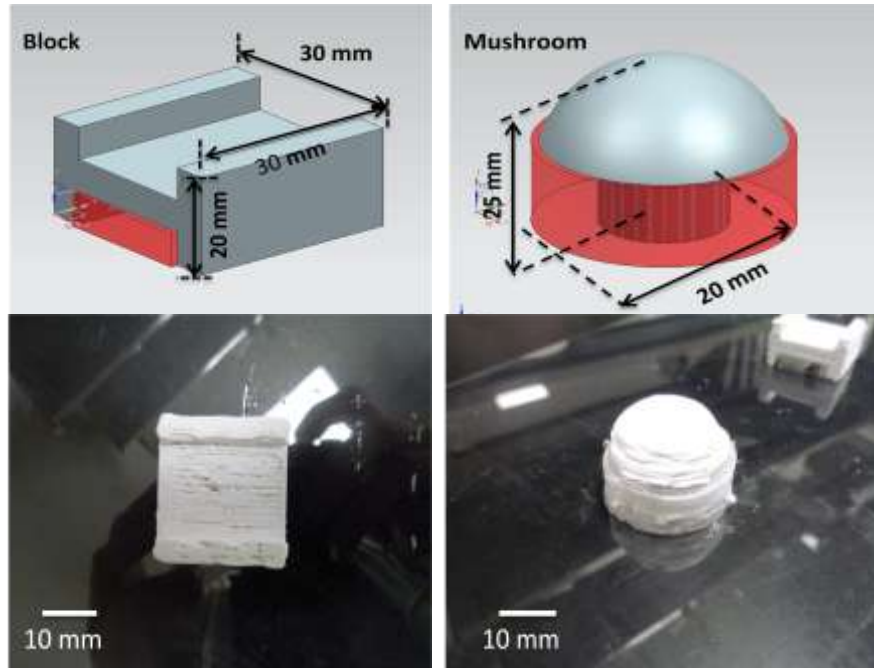wed that the minimum time for a 500 μm thick layer to freeze after reaching the 30th layer would be 10 s, during the part fabrication at -10° C using an alumina paste 45 vol. % solids loading. In the current experimental results, fabricating a part at freezing temperature of -10 °C with no waiting time between the layers would have difficulty of freezing the deposited layer after reaching the 25th layer (15 mm). A stand-off distance of 600 μm was used, and the fabricated part at the above condition is shown in Figure 4.3. The freezing of the layers after the 25th was not complete even after using a waiting time of 5 s in the next set of experiments. This is due to the lack of thermal conductivity between successively deposited layers. However, waiting 10 s between two successive layers provided

sufficient time to let the deposited layer fully freeze under free convection. The above

experiments were in agreement with the simulated results reported by Li et al. [23].

Therefore, a waiting time of 10 s was applied to all the parts fabricated using the FEF

triple extruder. Some of the successfully built parts with a waiting time of 10 s are shown

in Figure 4.4.
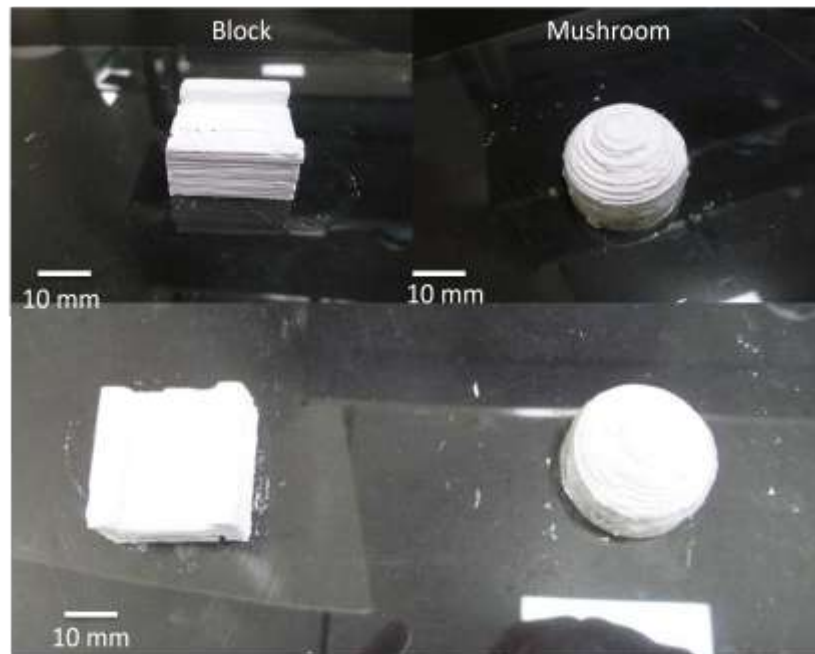
Figure 4.4. Extruded parts using FEF process with support materials using a waiting time of 10 s

A comparison of the quality of the parts fabricated with and without the waiting

time can be observed from Figures 4.3 and 4.4. The parts fabricated with a waiting time

of 10 s reveals a better surface finish after the 25th layer (Figure 4.4) when compared to

the parts made without any waiting time (Figure 4.3). As seen in Figure 4.4, the top part

of the block kept its straight edges without collapsing and the top of the mushroom

maintained its semi-spherical shape during the build.

Also, the layer height was reduced to 500 μm in the later experiments from previously used 600 μm. This provided a relatively better contouring and surface finish compared to the parts fabricated with 600 μm layer height. After adding the waiting time of 10 s and reducing the layer height from 600 μm to 500 μm, more parts requiring the use of support material were fabricated to compare the process quality. A part fabricated with this process can be seen in Figure 4.5.
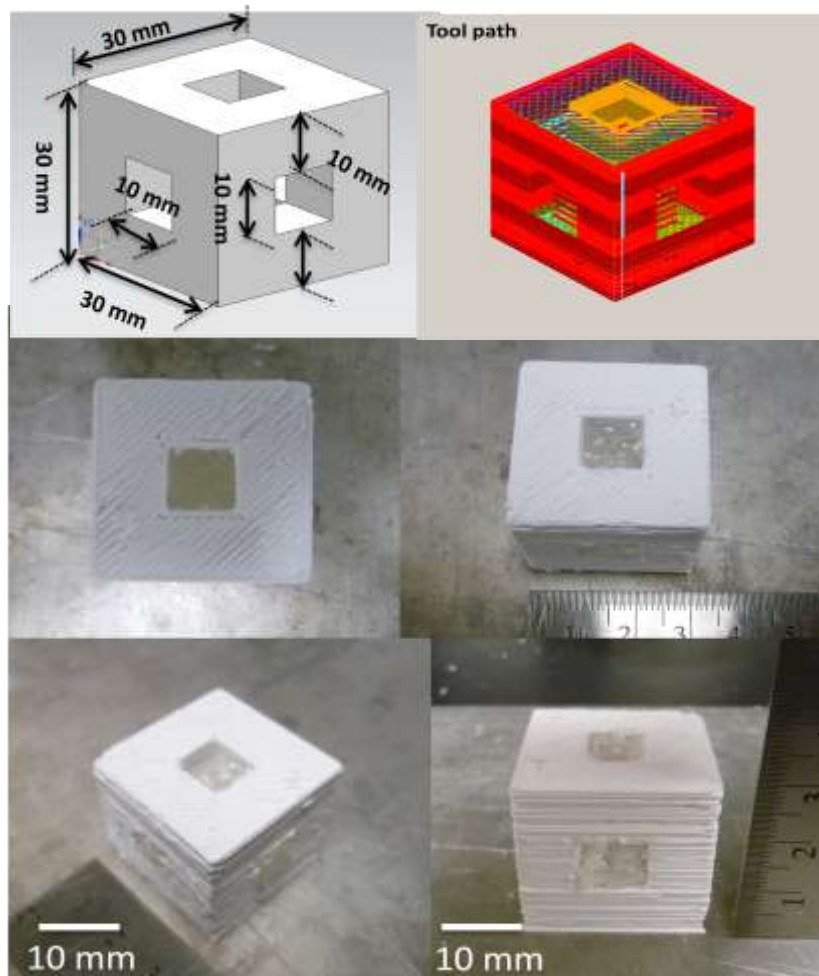
Figure 4.5. CAD model of a cube with square holes in each side and the extruded part with support material

In Figure 4.5 a cube with through square holes in all sides was fabricated to test the capabilities of the process. After the square holes from the sides were extruded with methyl cellulose, the top alumina layers were successively deposited and frozen without any collapse of deposited material. In Figure 4.6, a mushroom shape was fabricated again with a layer height of 500 µm this time to improve the surface compared to the mushroom in Figure 4.4.
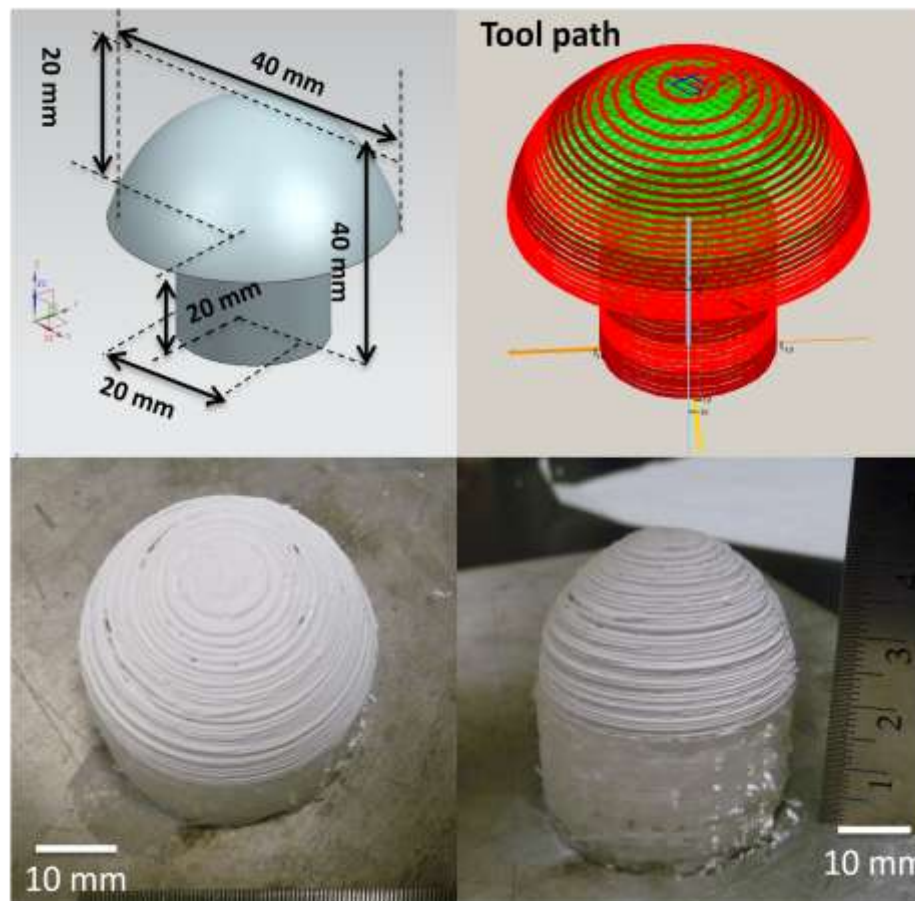
Figure 4.6. CAD model of a mushroom and the extruded part with methyl cellulose as support material

In the mushroom part (Figure 4.6), the part building time increased since the layer height is 500 μm compared to the previously of 600 μm. The bottom layer of the semi-sphere part of the mushroom did not show any deformation or collapse when depositing the paste by contouring for the semi-spherical portion of the mushroom.

In Figure 4.7, a complex Hilbert cube was extruded with overhangs and internal features in all sides. The process was capable of fabricating the cube completely, keeping its cubical shape without deformation.
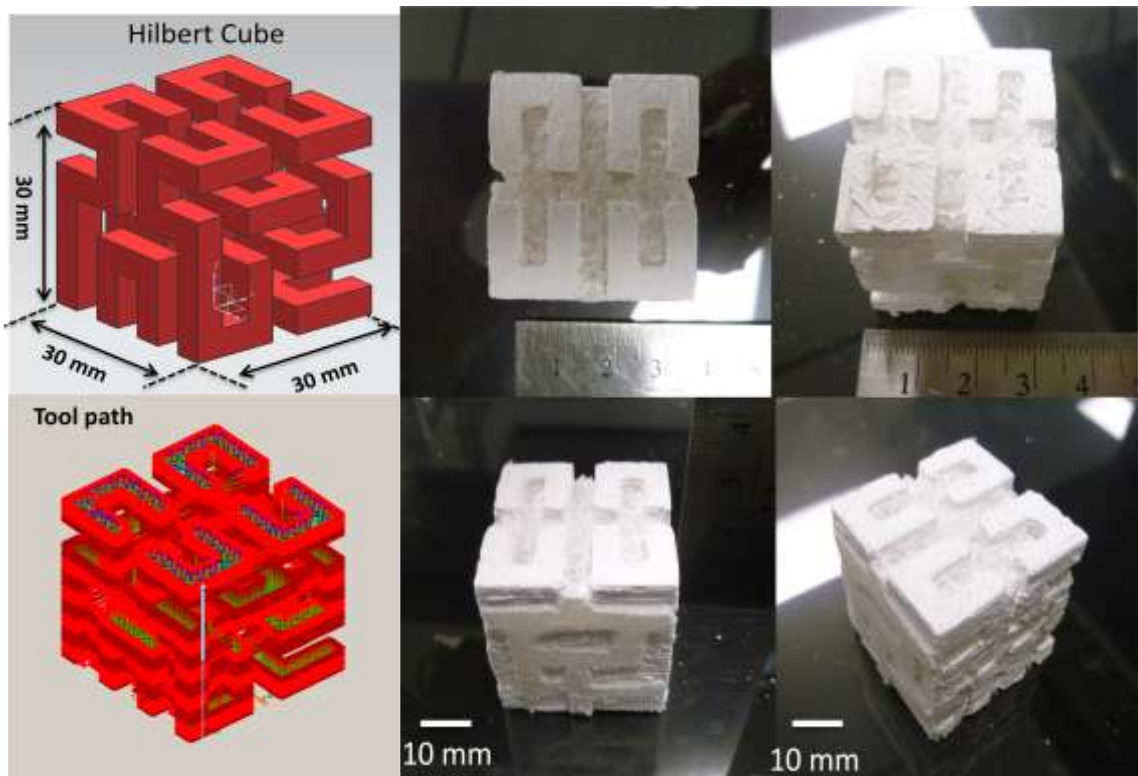
Figure 4.7. CAD model of Hilbert cube and the extruded part (viewed from different directions) with methyl cellulose as support material

4.2. DEBINDING AND SINTERING

Sintering is required to densify the alumina powder into a solid ceramic structure. Also, the methyl cellulose has to be burnt out to remove it from the part prior to sintering. The burnout and sintering schedule is shown in Figure 4.8.
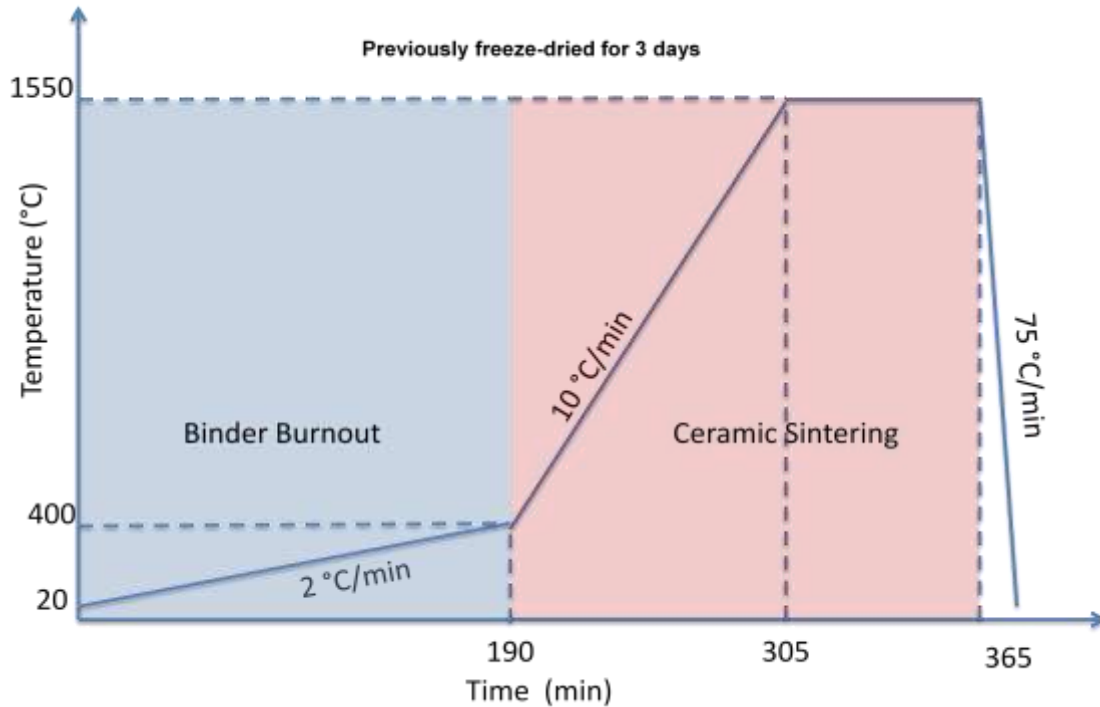
Figure 4.8. Sintering schedule after the part is made by the FEF process

The binder burnout process began slowly with a ramp of 2 °C/min and continued until reaching 400°C. During this time, the methyl cellulose was burned out. Then, the slope of ramp increased to a rate of 10°C/min until 1550 °C. After reaching 1550°C, the temperature was kept constant for one hour. By the end of that hour, the alumina had become a dense sintered part. Then, the furnace cooled down with a ramp of 75 °C/min until reaching room temperature. The slow ramp rate of 2 °C/min and the hold at 400 °C

were based on previous experiments in burning out organics out of ceramic bodies [16].

The most critical temperatures in the binder removal were obtained using

Thermogravimetric Analysis (TGA) to measure the weight loss of material as a function

of temperature. Based on the data collected from the TGA, the 10 °C /min until 1550 °C

and holding for an hour at that temperature were applied to sinter the alumina parts. The

results after sintering are shown in Figure 4.9
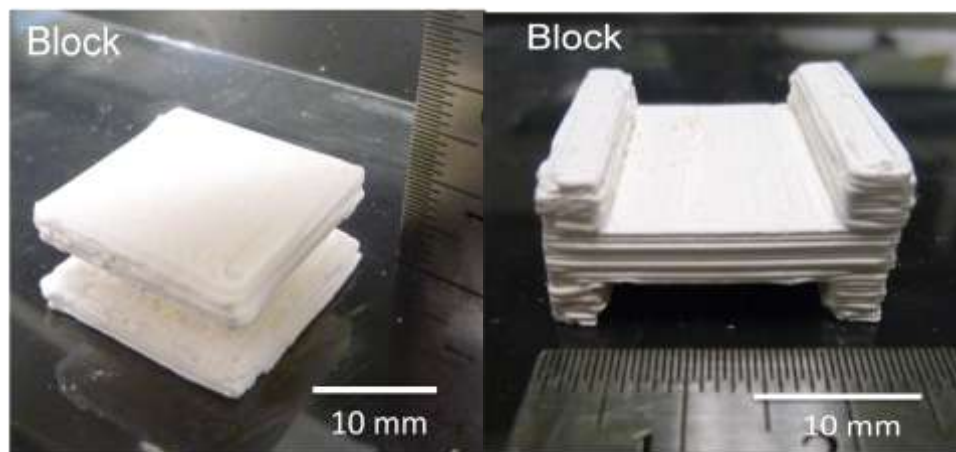
Figure 4.9. Two sintered parts with different geometrical shapes after sintering

The obtained parts indicated that the binder burnout schedule was sufficient to

remove the support material. Likewise, the increment in temperature from room

temperature to 1550°C to densify the ceramic part using the 2°C/min time was also

adequate to remove the remaining support material and to keep the ceramic part in its

original shape compared to its CAD model.

In Figure 4.10 and 4.11 the sintered mushroom and cube did not show any warping or deformation. Thus, the sintering schedule described was also suitable for parts of complex shapes.
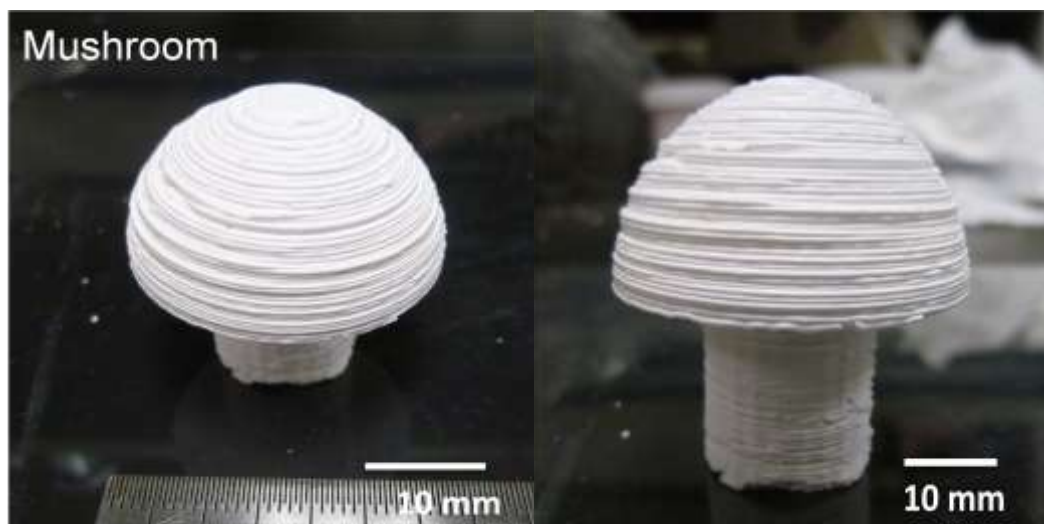
Figure 4.10. Sintered mushroom
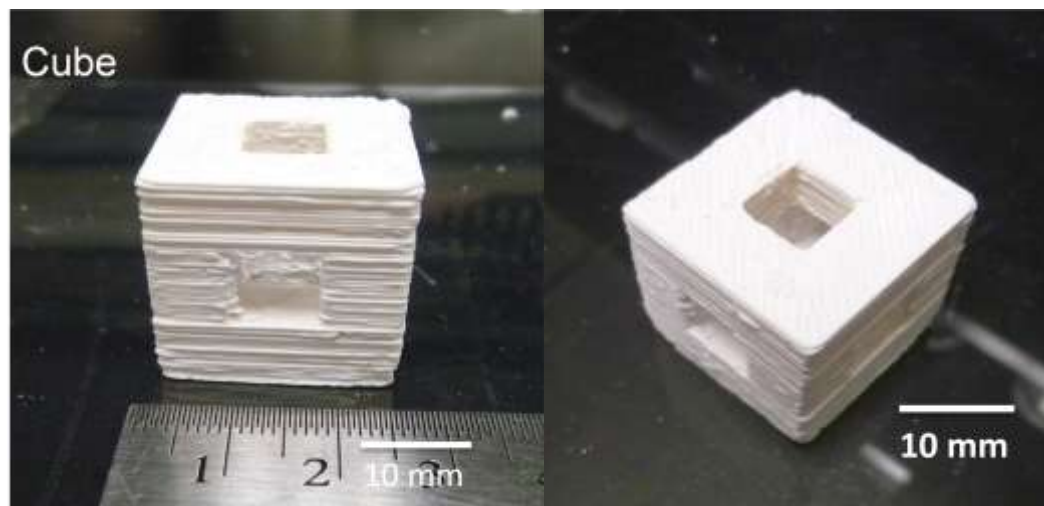
Figure 4.11. Sintered cube

4.3. PART ACCURACY

From the dimensions shown in Figures 4.12 and 4.13, part accuracy measurements were taken from the green state of the part using a caliper with a resolution of 1 μm. The objective of this experiment was to measure the part accuracy and shrinkage. The cube and mushroom were selected because their dimensions could be measured easily with a caliper. In Figures 4.12 and 4.13, each measured dimension is depicted with a letter.
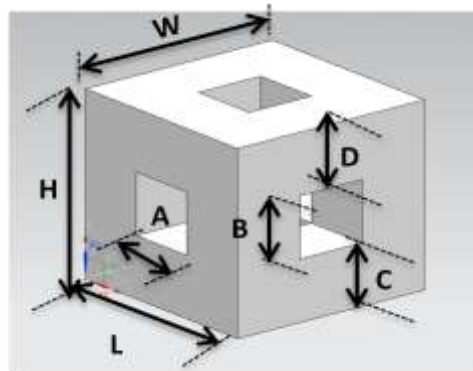
Figure 4.12. Dimensions to be measured for the cube-shaped part
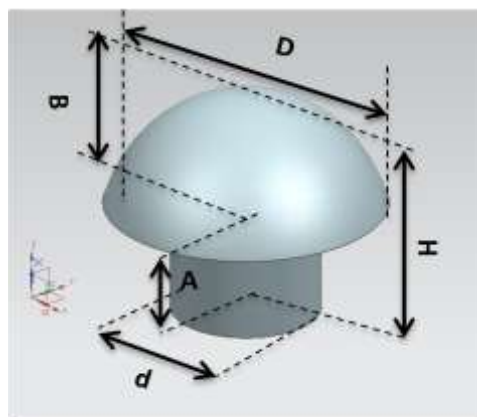
Figure 4.13. Dimensions to be measured for the mushroom-shaped part

Measurements from the cube and mushroom green parts were collected for various part dimensions shown in Figures 4.12 and 4.13, with four measurements per dimension taken randomly from the part. Table 4.1 shows the measurements with the means and standard deviations for the cube part.

Table 4.1. Measurements for a cube-shaped part in its green state

| Measurement	L(mm)	W(mm)	H(mm)	A(mm)	B(mm)	C(mm)	D(mm)
CAD model	30	30	30	10	10	10	10
1	30.20	30.10	30.17	10.10	10.20	10.6	11.0
2	29.81	29.88	29.87	9.90	9.60	0.97	9.80
3	29.75	30.40	30.23	9.80	9.80	0.90	9.20
4	30.40	29.95	29.80	11.00	1.10	0.96	9.90
Mean	30.04	30.08	30.01	10.20	10.10	9.70	9.90
Difference	0.04	0.08	0.1	0.20	0.10	0.30	0.10
% Difference	0.10	0.20	0.30	2.0	1.0	3.0	1.0
Standard Deviation	0.31	0.23	0.21	0.05	0.61	0.60	0.70

The percentage of accuracy between the CAD model and the green part for the cube varied from 0.3% to 3%. This difference was small and would suggest that the accuracy of the part made by the FEF process was good. This statement is also reinforced by the values of standard deviation (see Table 4.1). The standard deviations were relatively small compared to the CAD dimensions. The largest standard deviation was

0.31 for a dimension of 30 mm (0.3 %) and the largest standard deviation was 0.7 mm for a dimension of 10 mm in length (7%).

Table 4.2. Measurements for a mushroom-shaped part in its green state

Measurement	H (mm)	D(mm)	d(mm)	A(mm)	B(mm)
CAD model	40	20	20	20	20
1	40.3	39.9	19.85	20.41	20.52
2	40.15	39.45	19.73	20.23	20.32
3	39.97	39.85	20.10	19.96	20.33
4	40.25	39.40	20.19	19.87	19.97
Mean	40.16	39.65	19.96	20.11	20.28
Difference	0.30	0.10	0.04	0.11	0.28
% Difference	0.75	0.50	0.22	0.55	1.4
Standard Deviation	0.14	0.26	0.21	0.24	0.22

Table 4.2 shows the measurements with means and standard deviations for the mushroom part. In Table 4.2 the measurements taken for the mushroom also show that the percentage of accuracy between the green part dimensions and the CAD model dimensions vary from 0.75% to 1.4%. The mean standard deviation varied from 0.14 to 0.22. The standard deviation compared with the green part dimensions varied from 0.3% to 1%. The green part kept its shape well compared with the CAD model as can be seen in Figure 4.10.

Table 4.3. Measurements for the cube-shaped part after sintering

Test	L (mm)	W (mm)	H (mm)	A (mm)	B (mm)	C (mm)	D (mm)
1	25.19	25.11	25.09	7.96	7.74	7.87	7.77
2	25.09	25.07	24.88	7.90	7.65	7.80	7.70
3	24.92	25.02	25.12	7.84	7.82	7.74	7.82
4	25.30	24.87	24.97	8.04	7.80	7.90	7.86
5	25.15	24.92	25.00	7.84	7.82	7.92	7.84
6	25.07	24.87	24.77	7.94	7.76	7.88	7.92
7	24.96	25.13	25.06	7.90	7.90	7.79	7.84
8	25.82	25.08	24.80	8.00	7.82	7.91	7.78
Mean	25.18	25.00	24.96	7.92	7.78	7.85	7.81
Standard deviation	0.28	0.10	0.13	0.071	0.073	0.06	0.06
% Shrinkage	16	17	17	22	23	19	21

After sintering, the parts were measured 8 times different points for each dimension. Table 4.3 shows the measured results with means and standard deviations for the cube part after sintering. This table shows that the standard deviation varies from 0.7% to 1% and the percentage of shrinkage of the sintered part was in the range between 16% and 23% compared to the green part.

Table 4.4. Measurements for the mushroom-shaped part after sintering

Test	H (mm)	D (mm)	D (mm)	A (mm)	B (mm)
1	32.76	32.60	17.04	16.05	17.23
2	32.64	32.40	17.11	16.20	17.43
3	32.48	31.99	16.98	16.00	17.12
4	32.40	32.20	17.20	16.15	17.30
5	32.60	32.54	17.13	16.04	17.35
6	32.55	32.73	17.23	16.23	17.45
7	32.25	33.02	17.06	15.88	17.40
8	33.02	32.65	16.90	15.97	17.55
Average	32.58	32.51	17.08	16.06	17.35
Standard Deviation	0.23	0.32	0.11	0.120	0.13
% Shrinkage	19	18	14	20	14

Table 4.4 shows the measurements with means and standard deviation for the mushroom part after sintering. This table shows that the standard deviation varies from 0.7% to 0.74%, indicating that the quality of the green part was not affected after the sintering schedule since the range of % standard deviation is similar to its green state. The percentage of the shrinkage of the sintered part was in the range between 14% and 20% compared to the green part.

By comparing the CAD models and green parts, the developed FEF process was shown to have a dimensional accuracy of +/- 300 μm. This translates to +/-3% for the fabricated parts. The accuracy can be increased by using nozzles of smaller diameters,

though this also will increase the build time. For example, a nozzle of 300 µm can be

used in lieu of the current nozzle of 580 µm. In order to decrease the part building time

when using a smaller nozzle diameter, the extrusion force has to be increased, leading to

an increase in extrudate speed. Since the extrusion force was limited by the ram motor,

new hardware with more powerful motors will be needed in order to increase the

extrusion force.

5. CONCLUSIONS

A freeze-form extrusion fabrication (FEF) system with three extruders operating in a freezing environment (about -10 °C) has been developed and successfully implemented for building parts with complex geometries, using aqueous ceramic pastes as the main material and methyl cellulose as the sacrificial material. The process is environmentally friendly due to the use of a small amount of binder (2-10%) in the ceramic pastes of main and support materials compared to traditional additive manufacturing methods (binder ~40%) operating at room temperatures.

An empirical first-order dynamic model was used for the extrusion of alumina and methyl cellulose pastes to represent the dynamics with the ram velocity as the input and extrusion force as the output. A general tracking controller was applied to control the extrusion rate and also the starting and stopping of material extrusion for alumina and methyl cellulose. The controller reduced the time constant for both alumina and methyl cellulose pastes by ~65% when compared to the open-loop control system. The fabrication of 3D parts of different geometries with use of methyl cellulose as the support material demonstrated the capability of this process for fabricating complex shapes. The process accuracy was in the range of 300 μm for green parts compared to their CAD models. Shrinkage varying from 14% to 23% was recorded for the sintered parts when compared to the green parts. The sacrificial material was removed successfully from the final part during the binder burnout and sintering schedule. This process gave the final sintered part's internal features and overhangs which otherwise are difficult to fabricate using the previous FEF process.

BIBLIOGRAPHY

[1]   "Advanced Ceramics Technology Roadmap-Charting Our Course," Sponsored by U.S. Advanced Ceramic Association and U.S Department of Energy, Prepared by Energetics, Inc. and Richerson and Associates, December 2000.

[2]   S. Rangarajan, Q. Qi, N. Venkataraman, A. Safari, and S. C. Danforth, "Powder Processing, Rheology, and Mechanical Properties of Feedstock for Fused Deposition of Si3N4 Ceramics," *Journal of the American Ceramic Society*, *83*(7), pp. 1663-1669, 2000.

[3]   M. L. Griffith and J. W. Halloran, "Freeform Fabrication of Ceramics via Stereolithography," *Journal of the American Ceramic Society, 79*(10), pp. 2601–2608, 1996.

[4]   A. Bandyopadhyay, P. Panda, M. Agarwala, S. Danforth, and A. Safari, "Processing of Piezocomposites by Fused Deposition Technique," *Journal of the American Ceramic Society, 80*(6), pp. 1366-1372, 2000.

[5]   G. M. Lous, I. A. Cornejo, T. F. McNlty, A. Safari, and S. C Danforth, "Fabrication of Piezoelectric Ceramic/Polymer Composite Transducers Using Fused Deposition of Ceramics," *Journal of the American Ceramic Society, 83*(1), pp. 124-28, 2000.

[6]   A. Bandyopadhayay, R. K.Panda, V. F. Janas, M. K Agarwala, S. C. Danforth, and A. Safari, "Processing of Piezocomposites by Fused Deposition Technique," *Journal of the American Ceramic Society*, *80*(6), pp. 1366-72, 1997.

[7]   S. Danforth, Patent 5738817, April 14, 1998.

[8]   S. Crump, 3D Systems, Patent 5121329, June 9, 1992.

[9]   J. Cesarano III, R. Segalmen, and P. Calvert, P., "Robocasting Provides Moldless Fabrication from Slurry Deposition," *Ceramics Industry*, 148, pp. 94-102, 1998.

[10]   S. Crump, Apparatus and Method for Ceramic Three-Dimensional Objects, U.S. Patent No. 5121329, 1992.

[11]   J. W. Kietzman, A. G. Cooper, L. E. Weiss, L. Schultz, J. L. Lombardi, and F.B. Prinz, "Rapid Prototyping Ceramics Via Shape Deposition Manufacturing," Ph.D. Dissertation, Standford University, 1999.

[12]   J. A. Lewis, J. A. Smay, J. Stuecker, and J. Cesarano III, "Direct Ink Writing of Three-Dimensional Structures," *Journal of the American Ceramic Society, 89*(12), pp. 3599-3609, 2006.

[13]   G. Sui, "Modeling and Analysis of Rapid Freeze Prototyping," Ph.D. Dissertation, Missouri University of Science and Technology, Rolla, Missouri, 2002.

[14]   F. Bryant, G. Sui, and M. C. Leu, "A Study on the Effects of the Process Parameters in Rapid Freeze Prototyping," *Proceedings of the Solid Freeform Fabrication Symposium*, University of Texas at Austin, Austin, TX, August 5-7, 2002.

[15]   G. Sui and M. C. Leu, "Investigation of Layer Thickness and Surface Roughness in Rapid Freeze Prototyping," *ASME Journal of Manufacturing Science Engineering*, pp. 20-61, 2007.

[16]   T. Huang, M. S. Mason, X. Zhao, G. E. Hilmas, and M. C. Leu, "Aqueous-based Freeze-form Extrusion Fabrication of Alumina Components," *Rapid Prototyping Journal*, *15*(2), pp. 88 – 95, 2009.

[17]   X. Zhao, R. G. Landers, and M.C. Leu, "Experimental Investigation of Effect of Environment Temperature," *Proceedings of the Solid Freeform Fabrication Symposium*, University of Texas at Austin, Austin, TX, August 6-8, 2007.

[18]   X. Zhao, R. G. Landers, and M.C. Leu, "Adaptive-Control of Freeze-form Extrusion Fabrication Process," *ASME Journal of Manufacturing Science Engineering*, pp. 20-61, 2007.

[19]   T. Oakes, P. Kulkarni, R. G. Landers, and M. C. Leu, "Development of Extrusion on Demand for Ceramic Freeze Form Extrusion Fabrication Process," *Proceedings of the Solid Freeform Fabrication Symposium*, University of Texas at Austin, Austin, TX, August 9-10, 2009.

[20]   M. C. Leu, Q. Liu, and F. D. Bryant, "Study of Part Geometric Features and Support Materials in Rapid Freeze Prototyping," *Annals of the CIRP, 52*(1), pp. 185-188, 2003.

[21]   M. Li, Tang, L., Xue, F., and Landers, R.G., "Numerical Simulation of Ram Extrusion Process for Ceramic Materials," *Proceedings of Solid Freeform Symposium*, Austin, TX, pp. 290-308, 2011.

[22]   B. K. Deuser, M. Li, A. Thornton, L. Tang, R. G. Landers, M. C. Leu, and G. E. Hilmas, "Freeze-form Extrusion Fabrication of Three-Dimensional Functionally Graded Material Parts," *ASME Journal of Manufacturing Science and Engineering*, 2012.

[23]   M. Li, R. G. Landers and M. C. Leu, "Modeling, Analysis and Simulation of Paste Freezing in Freeze-form Extrusion Fabrication," *Proceedings of Solid Freeform Symposium*, Austin, TX, 2012.

[24]   C. S. Dewey, P. K. Lefforge, and G. L. Cabot, "Moisture Sorption by Carbon Black," *Industrial and Engineering Chemistry*, pp 1045-1050, 1932.

[25]   Herschel, W. H and Bulkley, R., "Consistency of measurements in rubber-benzene solutions," *Colloid Journal 39*, pp 291-300,1926.

APPENDIX

This appendix describes the use of the FEF triple extruder machine at Missouri S&T starting from generating a tool path for extrusion and then building the part under freezing conditions.

Machine Start-Up

1. To start the machine, turn on the PXI RT controller, and then turn on the two drives to enable control of the 6 motors.

2. Wait for the PXI RT controller to finish booting up. After booting up, open the program Measurement and Automation Explorer (MAX) provided by National Instruments.

3. In the program MAX you will find the following screen. Click on the PXI-7334 (1) and PXI-7334 (2) thumbnails to initialize them by pressing the button Initialize. This button will initialize the motion cards as shown in Figure A1.
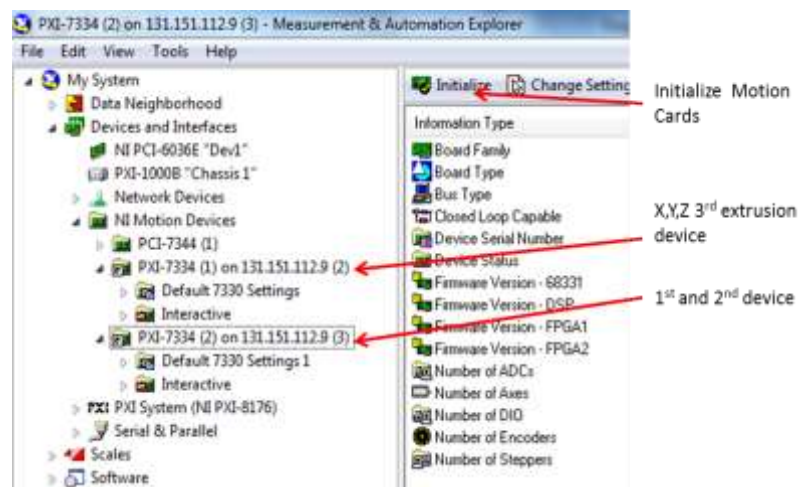
Figure A1. MAX program screen

4. Figure A2 explains the step-wise procedure to move the X-Y Z gantry system and the three extrusion devices. In PXI-7334 (1), axes 1, 2, 3, and 4 refer to Z, X, Y axes and the 3rd extrusion device, respectively. In PXI-7334 (2), axes 1 and 2 refer to the 1st and 2nd extrusion devices, respectively.
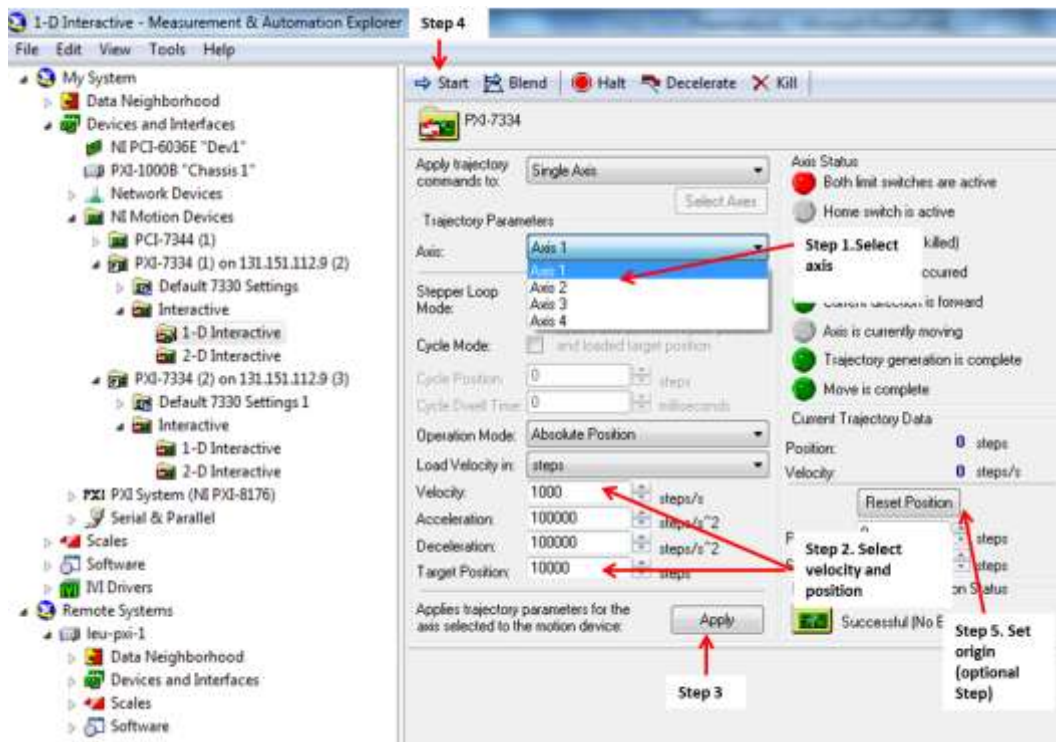

Figure A2. Step-wise directions to jog axes and extrusion devices

Generate G-Code

1. Generate an .STL file for the support and main materials using any CAD software.

2. Generate the tool path using Skeinforge software for both main and support materials.

3. Open the C++ converter program. In the program specify the G-code name.txt file and type it in the following line of code (Figure A3). In the final line of code name the file that will be converted to a Lab VIEW code (Figure A4).

```
{

ifstream fin("C:\\Diego\\BlockKCsupport.txt");//input 1
ofstream fout("C:\\Diego\\Block_1.txt");// middle output
string s;
string m101="101";
string m103="103";
string m;

cout<<" choose main or not(support)"<<endl;
string choose;
cin>>choose;
```

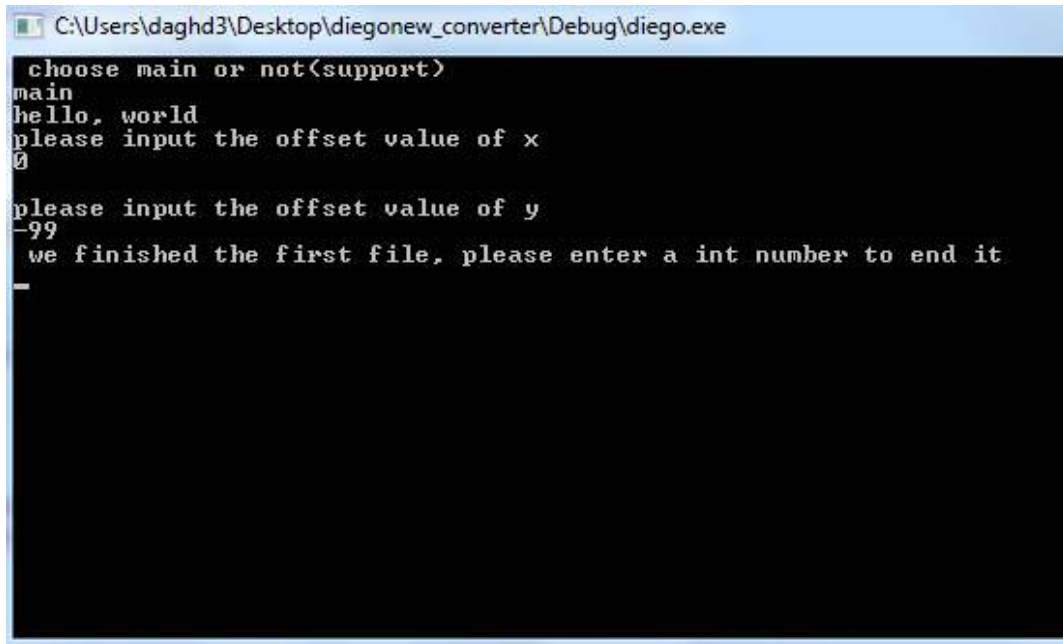Figure A3. Input name of G-code.txt file

```
ifstream fin2("C:\\Diego\\Block_1.txt");//middle output
ofstream fo2("C:\\Diego\\BlockKCsupport_final.txt");//final output1


string s_x;
string s_y;
string s_z;
string s_value;
```

Figure A4. Output name of LabView.txt file

4. When running the C++ program, the main or support material and the X and Y offsets can be specified as shown in Figure A5.

Figure A5. .exe window for the converter

5. Open the MATLAB program "Concatenate2.m" to merge the files for building

   main and support materials.

6. Open MAX explorer and click on the remote system PXI thumbnail. Then, right-

   click on it to select file transfer (Figure A6a). Transfer the file to the PXI
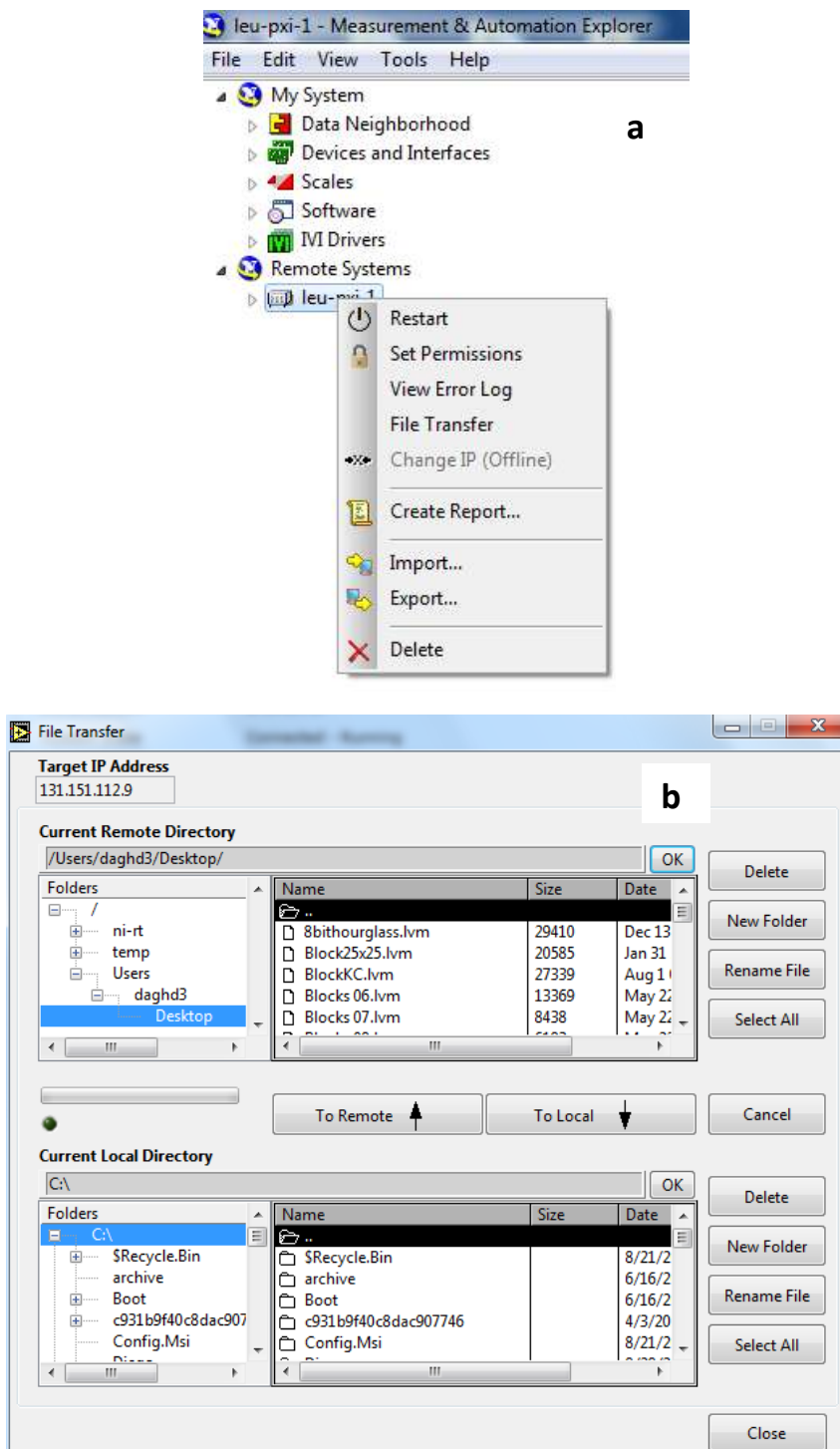
   destination folder (Figure A6b).

Figure A6. File transfer process to PXI controller

LabVIEW User Interface

1. Open the project "Extrusion plus motion.lvproj" and right-click on the PXI

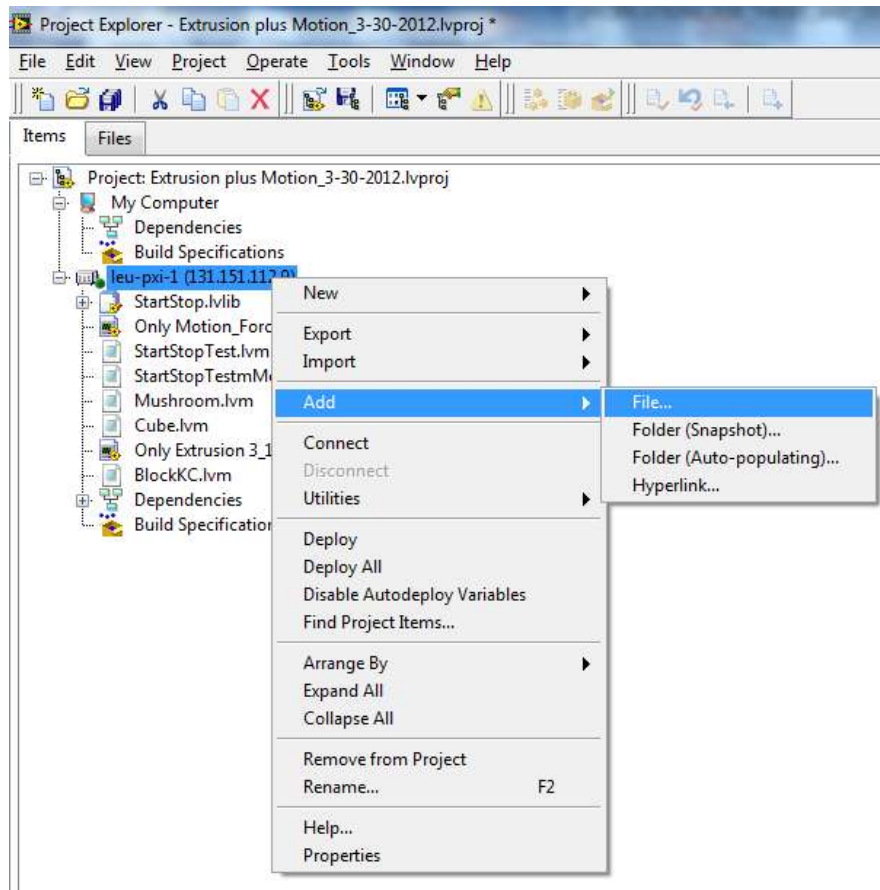   controller to add the tool path.lvm file to the project (Figure A7)

Figure A7. File addition to the project

2. Right-click on the PXI controller and deploy all the project including the .vi
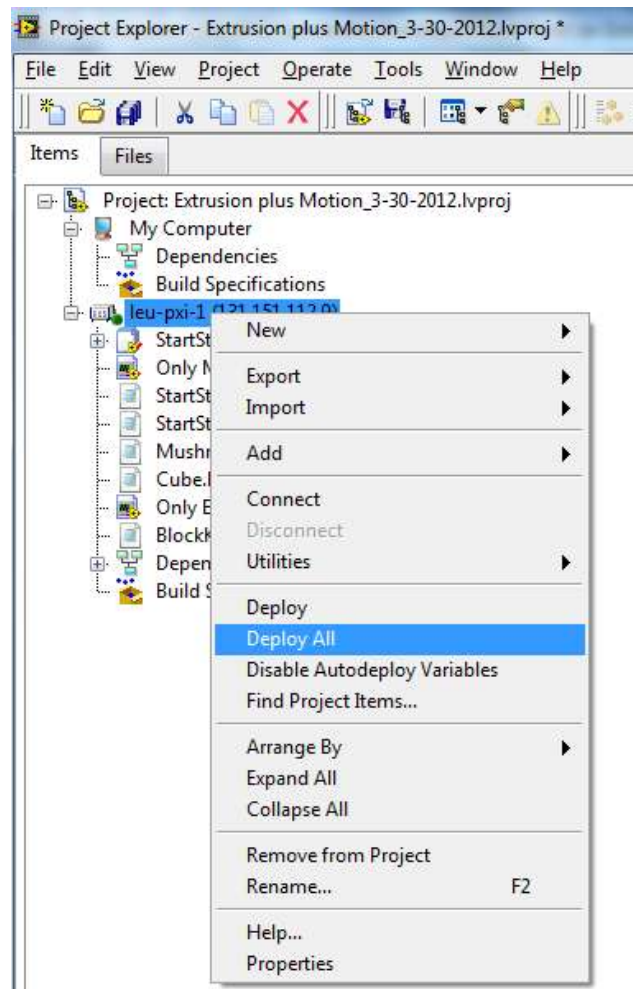
   programs and .lvm files (Figure A8).

Figure A8. Project deployment

3. Open the "Only extrusion.vi" and then enable the Force Controller to specify the

force values in Newtons to start and stop extrusion for the extrusion device 1 and
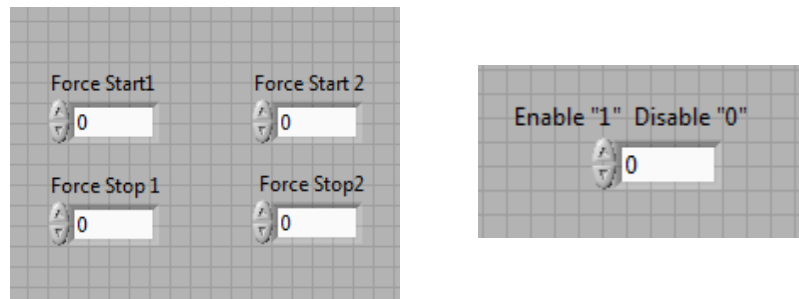
2. (Figure A9)

Figure A9. Project deployment

Note: To stop the "Only extrusion.vi" program, disable the force controller before stopping the whole program.

4. Open the "Only motion.vi", select the tool path.lvm file and specify the required table speed in mm/s.

VITA

Diego Armando Garcia Montaño was born in Cochabamba, Bolivia. In 2006, he received his Bachelor of Science degree in Electronics Engineering from Universidad Mayor de San Simon, Cochabamba, Bolivia.

Upon completing his undergraduate degree, he worked in Cochabamba city for the Engineering Department and in the automation industry for Tritec SRL Schneider Electric Systems Integrator and ABB Inc.

In August 2010, he began his studies for the Master of Science degree in Manufacturing Engineering. In December, 2012, he received his Master's degree in Manufacturing Engineering from Missouri University of Science and Technology. His areas of interest include manufacturing, controls, automation, robotics, and rapid prototyping.